

Project No. 12-3507

Uncertainty Quantification and Management for Multi-scale Nuclear Materials Modeling

Nuclear Energy Advanced Modeling and Simulation

David McDowell
Georgia Institute of Technology

In collaboration with:
None

Dan Funk, Federal POC
Laura Swiler, Technical POC

Final Report

September 1, 2012-August 31, 2015

CFP-12-3507: Uncertainty quantification and management for multiscale nuclear materials modeling
(NEAMS-3: Development of Phenomena-Based Methodology for Uncertainty Quantification)
PI: D.L. McDowell; co-PIs C. Deo, T. Zhu and Y. Wang, Georgia Tech

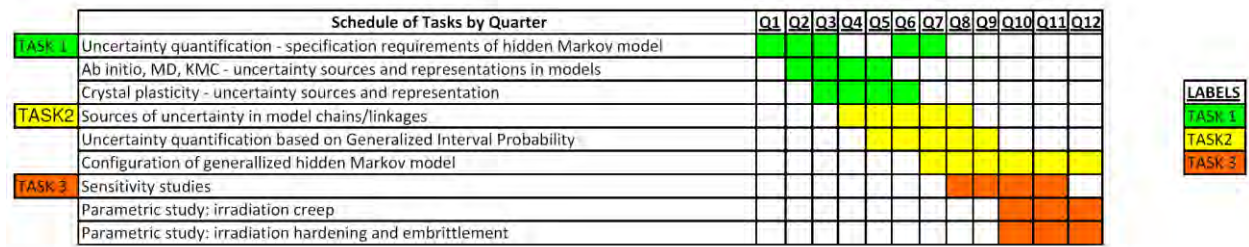
Table of Contents

Matrix of Faculty, Students, Tasks and Topics	2
Overall Program Rationale and Goals	3
Task 1. Uncertainty quantification – specification requirements of hidden Markov model.....	5
Task 1. Ab initio, MD, KMC – uncertainty sources and representation in models	5
Uncertainty Sub-Problems	6
UQ Method for Uncertainty Sub-problems	6
Task 1. Crystal plasticity – uncertainty sources and representation	28
Task 2 Sources of uncertainty in model chains/linkages: Uncertainty Sub-Problems.....	31
Task 2. Uncertainty quantification based on Generalized Interval Probability	37
Task 3 Sensitivity studies	41
Summary of Accomplishments, September 1, 2012 – August 31, 2015.....	42
Conferences Attended	42
Conference Presentations.....	43
Journal Articles.....	45
Theses Awarded.....	46
Invited Seminars	46
Conference, Symposium and Workshop Organization	47
May 8, 2014 Sandia Review of the Georgia Tech NEAMS Program.....	48
Quadchart	49
Suggested Future Directions	49
References	51

Matrix of Faculty, Students, Tasks and Topics

Primary Faculty Advisor(s)	Topic	Student
Ting Zhu	Atomistics and unit processes Informing crystal plasticity Informing KMC Uncertainty of interatomic potentials, boundary conditions, schemes, etc.	Zhi Zeng, Passed PhD proposal in Spring 2015; expected to graduate in Spring 2016.
Chaitanya Deo	KMC and event frequencies for mechanisms Uncertainty of events, frequencies, unit processes, interactions, etc. Informing crystal plasticity	Richard Hoffman – Passed PhD proposal in Fall 2015; expected to graduate in Fall 2016. Alex Moore, earned MS in 2014 and Passed PhD Proposal, expected to graduate in Summer 2016. Each partially supported.
David McDowell and Yan Wang	Crystal plasticity Hierarchical multiscale modeling chains Interval probability estimates and schemes Oversight and collaborative execution of uncertainty propagation and mitigation	Aaron Tallman, Passed PhD quals, will defend PhD proposal in November 2015; expected to graduate in Fall 2017. Joel Blumer, graduated with MS in Spring 2015.

This final report covers quarters 1-12 in the Gantt chart below.



Overall Program Rationale and Goals

Understanding and improving microstructural mechanical stability in metals and alloys is central to the development of high strength and high ductility materials for cladding and cores structures in advanced fast reactors. Design and enhancement of radiation-induced damage tolerant alloys are facilitated by better understanding the connection of various unit processes to collective responses in a multiscale model chain, including:

- dislocation nucleation, absorption and desorption at interfaces,
- vacancy production, radiation-induced segregation of Cr and Ni at *defect* clusters (point defect sinks) in BCC Fe-Cr ferritic/martensitic steels
- investigation of interaction of interstitials and vacancies with impurities (V, Nb, Ta, Mo, W, Al, Si, P, S)
- time evolution of swelling (cluster growth) phenomena of irradiated materials
- energetics and kinetics of dislocation bypass of defects formed by interstitial clustering and formation of prismatic loops, informing statistical models of continuum character with regard to processes of dislocation glide, vacancy agglomeration and swelling, climb and cross slip.

In view of the obvious complexity of the mechanisms involved and approximations made in modeling necessitated by the disparity in length and time scale of applications with modeling and simulation, as well as limited number of physical experiments, uncertainty comes to the fore as consideration in application of such schema. This research program has focused on quantifying and managing uncertainty in multiscale modeling of the inelastic behavior of BCC Fe-Cr ferritic/martensitic steels at ambient and elevated temperatures as affected by irradiation damage, using a framework connecting atomistics, kinetic Monte Carlo

and a coupled crystal plasticity-point defect rate theory model. The primary platform is a multiscale modeling framework that includes first principles and atomistic simulations of knock-on events with regard to remnant vacancy and interstitial fields and loop defects, the influence of interstitials on dislocation core spreading and mobility, Metropolis Monte Carlo and kinetic Monte Carlo (kMC) studies of collective unit processes to accumulate damage over higher length and time scales at elevated

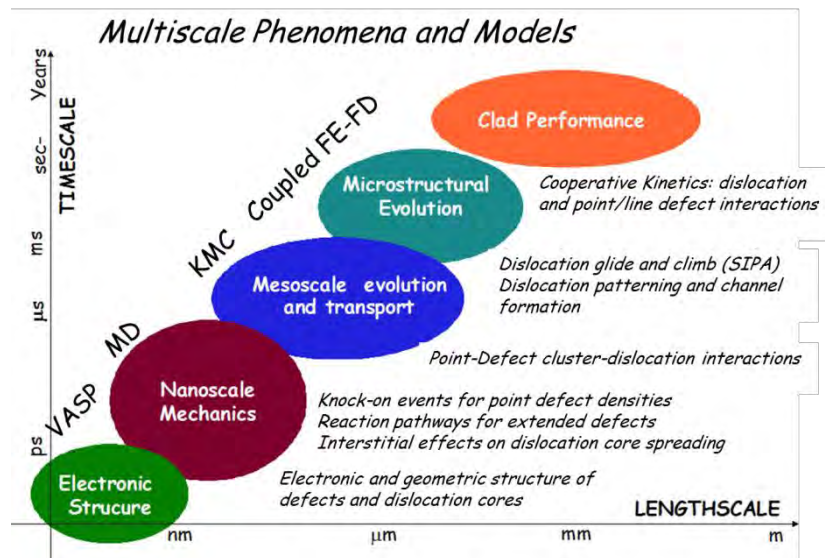


Fig. 1: Multiscale processes and models that govern irradiation damage, defect clusters, and defect-dislocation interactions relevant to ambient and elevated temperature plasticity phenomena in structural materials in advanced reactors. Coupled FE-FD pertains to continuum crystal plasticity models.

temperatures that are relevant to structures in service in the cladding and core assembly of advanced reactors, and a continuum crystal plasticity model that couples point defect and dislocation production/annihilation/migration, considering interaction with interstitial loops. Figure 1 illustrates various levels of the hierarchy of mechanisms and associated models.

The goal of this three-year program was to establish a consistent methodology to quantify uncertainty in model parameter and inputs/assumptions, as well as numerical implementation, and to develop a means to consider:

- Uncertainty quantification in each model
- Propagation of uncertainty in multiscale model chains
- Sensitivity studies and parametric evaluation of uncertainty on model problems.

After the first year of the program, and in accordance with feedback from our technical monitor Dr. Laura Swiler, in October 2013 we consolidated the focus of the program to a set of three multiscale uncertainty sub-problems exercising different physical mechanisms and modeling and simulation aspects of the multiscale model chain in Fig. 1:

1. Interstitial Loop/Dislocation Interactions in Irradiated Fe Alloys
2. Void Nucleation, Growth and Interactions with Dislocations in Irradiated Fe Alloys
3. Bottom-Up and Top-Down Uncertainty in Informing Crystal Plasticity for BCC Systems

These sub-problems were carefully defined and mapped to exploit the connectivity of underlying *ab initio*, MD, KMC and crystal plasticity modeling in multiscale modeling chains. This strategy refocused the parametric studies in Task 3 to be directed towards parametric sensitivity studies and corresponding uncertainty quantification and propagation in these critically important mechanisms and elements of multiscale model chain. Initial program focus on feasibility studies of the Generalized Interval Bayes' Rule (GIBR) in terms of shedding new light and capabilities on uncertainty in multiscale model chains culminated in the MS Thesis of Joel Blumer. It was found that the GIBR has potential but is somewhat limited in its imposition of useful bounds for behavior in the classes of discrete and continuous multiscale models addressed in our three uncertainty sub-problems. It remained a subject of inquiry in this program, but a desire to maintain focus on uncertainty propagation and mitigation in these three sub-problems drew the focus towards pursuit of uncertainty quantification using classical latin hypercube sampling and polynomial regression modeling, while maintaining the overall objectives of addressing complex multiscale phenomena in irradiated Fe-based alloys. Work in the last year of the program (and continuing work in closure of the PhD theses based on this program) pursued this route on the three uncertainty sub-problems, in essence supporting these parametric studies listed in Task 3

This program has produced novel approaches to quantifying uncertainty and its propagation across multiple models exercised to reflect physical phenomena occurring at vastly different length and time scales (from sub-nm (atoms) to tens of microns (polycrystals)) and has spurred visibility of the field of multiscale uncertainty in the broader basic materials research community and the broader Materials Genome Initiative. It has supported the thesis work of 5 graduate students, one completed MS thesis (4 PhD dissertations in-progress), and has involved:

- 4 journal articles published, 1 submitted, 9 in preparation
- 20 conference presentations
- 1 MS thesis, several PhD theses in progress

Faculty in this program have delivered five related invited seminars, and organized or co-organized five conferences and symposia organized related to multiscale modeling and uncertainty.

Task 1. Uncertainty quantification – specification requirements of hidden Markov model

All elements of Task 1 were completed in Q7, on schedule.

In accordance with feedback from our technical monitor Dr. Laura Swiler, we consolidated the sub-problem definition in October 2013 to a series of three multiscale uncertainty sub-problems to achieve more focus. These sub-problems were defined and mapped to exploit the connectivity of underlying ab initio, MD, KMC and crystal plasticity modeling in multiscale modeling chains:

1. **Interstitial Loop/Dislocation Interactions in Irradiated Fe Alloys**
2. **Void Nucleation, Growth and Interactions with Dislocations in Irradiated Fe Alloys**
3. **Bottom-Up and Top-Down Uncertainty in Informing Crystal Plasticity for BCC Systems**

Task 1. Ab initio, MD, KMC – uncertainty sources and representation in models

This sub-task was completed in Q5 (October – December 2013). We next present the mappings for first principles, MD and KMC models with in uncertainty sub-problems, along with model chains /linkages that were part of the Task 2 effort.

Sources of Epistemic Uncertainties in Multiscale Modeling & Simulation

All models require certain levels of abstraction; hence, approximation error is inevitable. The causes of these errors are the major sources of epistemic uncertainties in modeling and simulation (M&S). Epistemic uncertainty in M&S is also referred to as model form uncertainty.

In density functional theory (DFT), the major source of model form uncertainty or error is the exchange-correlation potential functionals, where many-particle interaction is approximated and simplified. In addition, the pseudopotentials are typically used to replace the Coulomb potential near each nucleus in the calculation, which also introduces numerical error. In the self-consistency calculation of ground state energy, the chosen threshold for convergence also introduces numerical error.

In molecular dynamics (MD) simulations, the major source of model form and parameter uncertainties is the uncertainty associated with the interatomic potential function. As the input of MD, the approximation error is naturally propagated to the output prediction through the simulation process. Other sources of uncertainties include the cut-off distance in simulation for ease of computation, the imposed boundary conditions that may introduce artificial effects, simulation acceleration through modified potentials or the application of physically unrealistic high strain rates which is to overcome the time scale limitation of MD, the computational error with different computer architectures because of round-offs in floating-point numbers or task distribution and sequencing in parallel computation, the systematic error in measurement data that are used in model calibration, as well as other unknown biases introduced in building the models.

In kinetic Monte Carlo (KMC) simulations, the major sources of epistemic uncertainties are the incomplete event catalog and imprecise rates or propensities. The accuracy of KMC simulation depends on the validity of complete knowledge of all possible events. Furthermore, the true rates in physical world can vary along time. They are also dependent on the state of the system. For instance, external loads can change the diffusion of defects. Crowding effect exists in reactions where molecules easily block reaction channels. In KMC, events are also assumed to be independent for the convenience of computation. In reality, they may be correlated. The unknown correlation between events is another source of uncertainty.

In summary, unknown bias and numerical treatment of any model in simulation introduce epistemic uncertainty into the model. As a result, the prediction as the simulation output is inherently imprecise. When macroscopic quantities as statistical ensembles are of our interest, the output is also inaccurate. Therefore, the simulation output contains both epistemic and aleatory uncertainties. Quantification of these uncertainties is necessary to improve the robustness of simulation prediction.

Uncertainty Sub-Problems

Y. Wang and D.L. McDowell co-advised PhD student Aaron Tallman, who collaborated with co-advised MS student Joel Blumer to chart out the flow of information in uncertainty sub-problems as a major collaborative effort within Task 1 of the project.

First we discuss the UQ approach for these uncertainty sub-problems, followed by a discussion of modeling and simulations characteristic of each.

UQ Method for Uncertainty Sub-problems

We will describe application of the Generalized Interval Probability Method later in this report, with reference to the combined bottom-up/top-down crystal plasticity uncertainty sub-problem #3. Here we describe the overall UQ strategy taken for the systematic treatment of all three uncertainty sub-problems within the context of the doctoral theses of the students supported by this NEAMS program over the past three years.

Assumptions associated with the UQ approach are clarified, starting at a philosophical level and continuing through the execution of the procedure [1-7].

- 1) Identification of a Candidate model: The scientific model that will be used for this approach must have certain features, but otherwise it can have any form. The model must allow being calibrated to data, ideally by the adjustment of calibration parameters. It must be possible for one or more of these calibration parameters to be re-interpreted as physical parameters whose values are determined by a separate model.
- 2) Construction of the Black Box: The model must be given a black box treatment. The scientific model as a whole can be considered as a combination of scientific theory and an empirical calibration. The hypothesis that will be tested in this procedure is only linked to the theoretical component of the model. However, the calibration parameters that inform the model may have theoretical limits to their values. These limits should be identified. The structural part of the model is then analyzed only by its behavior, as one would a black box model. This is to aid comparison of models of diverse classes which seek to describe or connect the same phenomena. The prior likelihood in the calibration space is assumed to be a uniform density across the structurally bound values.

- 3) Initial Sampling of Calibration Space: A polynomial regression on the calibration parameters to the Loss functions cannot be made without an initial sampling of the model across the calibration space. This sampling should be designed to minimize extrapolation, and should contain enough points to support the construction of the regression model of at least 2nd degree.
- 4) Per Datum Loss Functions from Likelihood: The value of $(y^e - y^m) / \sigma^e$ experimental response less model response divided by experimental std. dev. is linked to calibration space using a regression model for each datum. The composite likelihood-based objective function:

$$\exp\left(\frac{-1}{2} \sum_i [f_i(\boldsymbol{\theta})^2]\right)$$

is defined, where i represents which datum, f is the per datum loss function of $\boldsymbol{\theta}$, the calibration space of the model. This form is a reflection of the per datum likelihood of the model according to a Gaussian model of experimental errors. The per datum likelihoods are included together to reflect the hypothesis that the model is true for all data used. The pre-exponential portion of the likelihood is not included. This is because the regression functions are not one-to-one mappings.

- 5) Mismatch of model structure from data as yardstick for level of discrimination in calibration space: The Maximum Likelihood Estimate or MLE of the model calibration parameters can be found by maximizing the objective function above. This calibration of the model reflects the closest approximation of the data that can be made within the constraints of the theory-informed model structure. Given that this approach is an attempt to measure the uncertainty associated with the model structure, the limitation of the structure (in the model's inability to exactly match the observed data) is a crucial measurement. In cases where the data based objective function value of the MLE is less than $\exp(-\frac{1}{2})$, a new term σ_{str} is added to the objective function:

$$\text{Obj}(\boldsymbol{\theta}) = A \cdot \exp\left(-\frac{1}{2\sigma_{str}^2} \sum_{i=1}^n [f_i(\boldsymbol{\theta})^2]\right)$$

The value of σ_{str} is determined such that at the MLE (for which $\boldsymbol{\theta} = \hat{\boldsymbol{\theta}}$):

$$\sigma_{str}^2 = \sum_{i=1}^n [f_i(\hat{\boldsymbol{\theta}})^2]$$

The value A is a normalizing coefficient which is evaluated after σ_{str} is determined, such that:

$$\int_{\boldsymbol{\theta}\text{-space}} \text{Obj}(\boldsymbol{\theta}) = 1$$

In this way, the likelihood-based objective function restricts the calibration space to values supported by experimental observations, to a degree which is reflective of the comparative mismatch to data of different calibrations of the model. This is an approach to the problem of overfitting in models, where a model's calibration parameters are given values that compensate for structural shortcomings of the model [4].

- 6) Likelihood estimate across theoretically bounded calibration parameter space as a top-down structural uncertainty measurement: The resulting density function of the calibration space can be sampled or otherwise analyzed to find a measure of the uncertainty that remains in the structural

model after a calibration. Importantly, the calibration used here is not a classical deterministic calibration, where the MLE values for the calibration parameters might be chosen. Instead, this process prevents an overfitting-type situation from arising, i.e. where choices for parameter values are forced to compensate for inadequacies in the model structure. It prevents this by limiting the narrowness of the objective function with a structural variance term. The error or “distance” between the experimental response and the MLE calibrated model response is used as a yardstick in determining the likelihood ratios of different calibrations of the model.

- 7) Loss function in calibration space: A loss function is defined in calibration parameter space to describe the extent to which the model can connect response data (via calibration) to different points in calibration space. The form of the function is taken from ordinary least squares approaches.

$$\text{Loss}(\boldsymbol{\theta}^*) = \int_{\boldsymbol{\theta}\text{-space}} \text{Obj}(\boldsymbol{\theta}) \cdot \sum_j^{\theta_j \in \boldsymbol{\theta}} (\theta_j^* - \theta_j)^2 d\boldsymbol{\theta}$$

$\boldsymbol{\theta}^*$ is the value of the calibration parameters given from a bottom up model or elsewhere which is to be evaluated as the connecting data. The values for $\boldsymbol{\theta}$ should be normalized for the above equation such that for any calibration parameter j , $\inf(\theta_j) = 0$, and $\sup(\theta_j) = 1$.

- 8) Single Bottom-up model (without BU calibration) case, $\theta \rightarrow x$ discrepancy: In the case where a single bottom-up model seeks to inform the calibration parameter values for the model in the black box, the bottom-up model is first assumed to be inflexible. This situation can arise if the bottom-up model cannot be calibrated or if the model results are the only information available. In this situation, a top-down and bottom-up uncertainty measure cannot be made. Instead, a linkage can be analyzed in terms of the amount of discrepancy that accompanies reinterpreting calibration parameters in the mesoscale model as physical parameters determined by a bottom scale model. This discrepancy can be found using the loss function described in 7). The discrepancy measure can be compared to the value of the loss function for other cases, such as the self-discrepancy (for $\theta \rightarrow \hat{\theta}$ or MLE as connecting data), and the prior discrepancy, measured by replacing the objective function with a constant value (reflecting a uniform density in calibration parameter space). The prior self-discrepancy may be useful for identifying the effects of the calibration boundaries on the loss function.
- a. Care in interpreting the results here must be taken: if the calibration boundaries are set too narrowly, prior discrepancy measures may be lower than posterior measures even when a moderate connection is present. This can easily happen if model precedents are used to estimate bounds. Care must be taken to ensure that calibrations of past models do not inform these limits, which are ideally structural (pre-calibration) and theoretical in nature. If for example, a survey of calibrated models were used to inform calibration parameter limits, the prior uniform distribution on this calibration parameter space would reflect an estimate that has already been informed by calibrations, and it would not reflect a prior that is free from information not present and defined by the model’s theoretical structure.
- 9) Multi (or with calibration) Bottom-up case, TDBU structural uncertainty: In the case where the bottom scale model is flexible, or if multiple calibrations of the model are given, the structure of the bottom scale model can be included in the uncertainty measurement. For the case of the multiple point estimates, each point can be given a density that corresponds to the objective function below, based on the calibration space loss function from 7).

$$\text{Obj}(\boldsymbol{\theta}_k^*) = A \cdot \exp(-\text{Loss}(\boldsymbol{\theta}_k^*))$$

Here A is a normalizing coefficient valued such that the sum of the objective function values is 1 for the domain of $\boldsymbol{\theta}^*$.

If the bottom scale model can be calibrated in the analysis, the procedure of steps 1-6 can be reiterated on the bottom scale model -- describing the bottom scale model as a black box as well. The single loss function in mesoscale calibration parameter space takes the place of the per datum loss functions of step 4, in addition to those of data on the length scale of this second model. This places more of a burden on the regression model, so a more complicated treatment might be necessary to capture the relationship to a sufficient level of fidelity. Once the objective function is defined on the bottom scale calibration parameter space, a sampling method may be used with resampling at the mesoscale model to give a representation of the Top-down bottom-up uncertainty of the model chain structure.

- a. This may also be considered as a method for multiscale model calibration.

1. Interstitial Loop/Dislocation Interactions in Irradiated Fe Alloys

Two papers are planned for this sub-problem. One paper will be an uncertainty propagation analysis of the MD to crystal plasticity treatment of self-interstitial atom loops focusing on the uncertainty related to the choice of interatomic potential. The second paper will be a Top-down and bottom-up (TDBU) uncertainty analysis, applying the iterative approach described above

a) Black box model

Irradiation defect Crystal Plasticity model (modified from Patra and McDowell 2013) with a Friedel Kroupa Hirsch hardening treatment

b) Bottom-up information (parameter scale data)

Atomistic simulation of interstitial loop – dislocation interactions (Zhi Zeng) in terms of critical resolved shear stress to pass through the loop

c) Top-down information (output scale data)

Irradiation effects on hardening behavior (Maloy et al 2001)

d) Key calibration parameters of the model

Obstacle strength of interstitial loops as function of loop size and relative orientation (formulation TBD)

2. Void Nucleation, Growth and Interactions with Dislocations in Irradiated Fe Alloys

Two papers are planned for this sub-problem as well. The first will be a TDBU uncertainty analysis of multiple rate law models for void nucleation and growth. Following that analysis, a second paper will include an uncertainty propagation analysis through a crystal plasticity model.

3. Bottom-Up and Top-Down Uncertainty in Informing Crystal Plasticity for BCC Systems

Two papers have been planned. One paper will demonstrate and document the structural uncertainty quantification process detailed above, using the sub-problem as an example. An additional paper will incorporate work from Hale et al in order to test the ability of the approach to quantify the relative quality of scale bridging of one model chain to another.

Sub-problem 1: Interstitial Loop/Dislocation Interactions in Irradiated Fe Alloys

Students: Zhi Zeng and Aaron Tallman

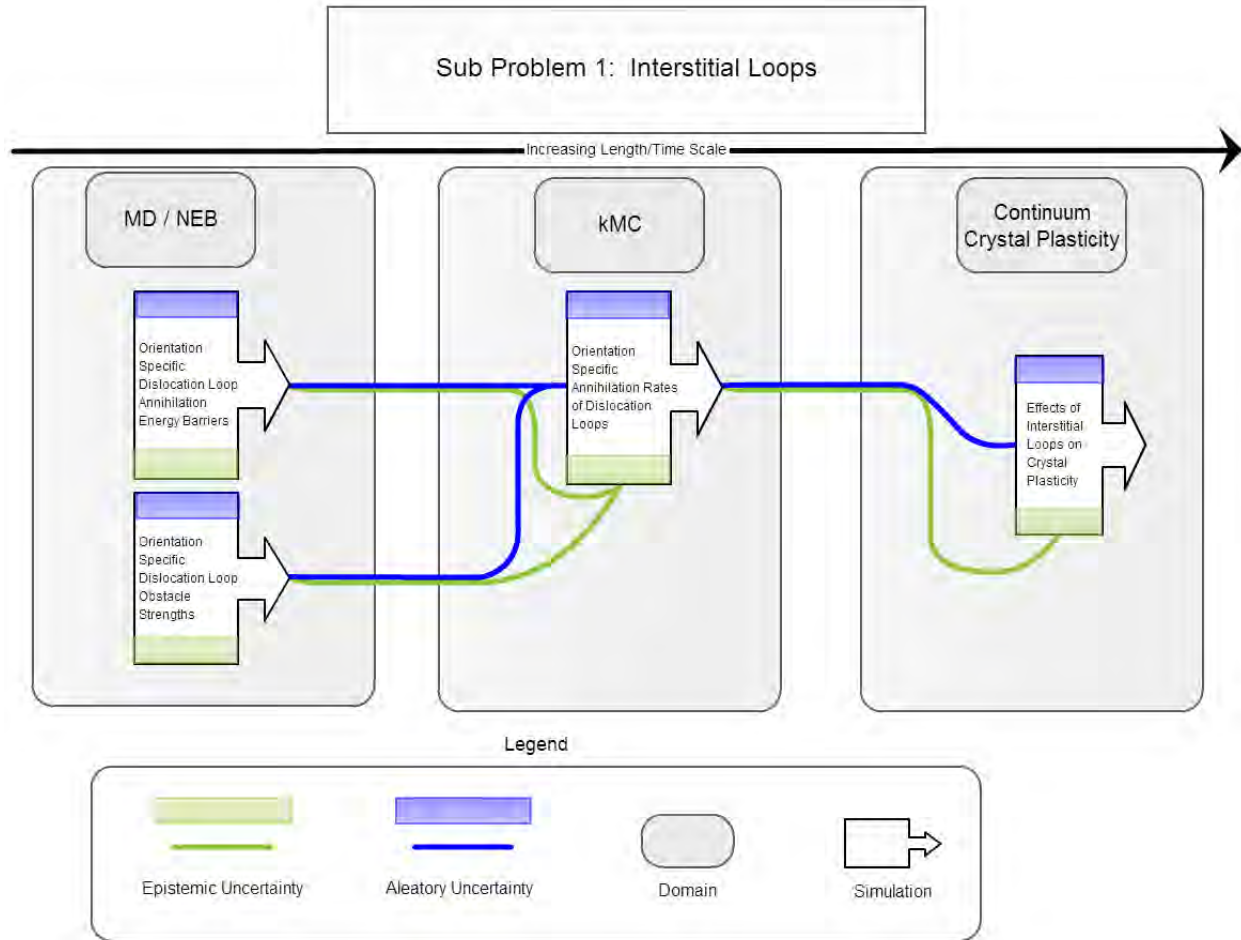
Faculty: Ting Zhu, David McDowell, and Yan Wang

Interstitial Loops have been found in irradiated BCC Fe alloys, and provide barriers to dislocation glide, and therefore plastic deformation. As the nature of these loops is explored, there is evidence that there are likely two distinct types of these loops. One type is found to be predominantly glissile and tends towards a hexagon in the $\{110\}$ planes, with a Burgers vector in the $1/2\langle 111 \rangle$ direction. The other type seems to be sessile, and is organized on $\{100\}$ planes in squares with burgers vectors of $\langle 100 \rangle$. These are distinct types which might be formed through separate mechanisms. The two types are thought to also have different barrier strengths. Work in this sub-problem is examining the pathways for the formation, annihilation, and displacement of interstitial loops, with the intent to inform continuum level models of crystal plasticity with regard to softening and strain localization.

The clearing of ostensibly sessile interstitial loops formed by aggregation of interstitials arising from knock-on events by virtue of interactions with mobile dislocations is a precursor to forming defect free channels that localize slip, lead to irradiation hardening, and compromise ductility of polycrystalline Fe-Cr alloys. The current crystal plasticity model used at higher length scales assumes annihilation of loops interacting with mobile dislocations within some capture radius, but the mechanisms are unknown and the rate equations have significant model form uncertainty. This includes the accounting for exchange of immobile and mobile dislocations within the dislocation density evolution equations of crystal plasticity.

Simulations models were identified as follows:

1. MD/NEB simulation of interstitial loop annihilation by orientation to dislocation to determine energy barrier of the annihilation
2. MD/NEB simulation of interstitial loop annihilation by orientation to dislocation to determine obstacle strength to dislocation motion
3. The incorporation of the data from the lower length scale models into Continuum Crystal Plasticity model



Three collaborative journal articles are planned as an outcome of this sub-problem:

1. **Uncertainty Propagation within MD-informed Crystal Plasticity Modeling of Mobile and Immobile Interstitial Loops in Irradiated bcc Fe**
Zhi Zeng, Aaron Tallman, Ting Zhu, Yan Wang, David L. McDowell
2. **Top-Down and Bottom-Up Uncertainty Quantification of MD-informed Crystal Plasticity Modeling of Mobile and Immobile Interstitial Loops in Irradiated bcc Fe**
Aaron Tallman, Zhi Zeng, Ting Zhu, Yan Wang, David L. McDowell
3. **Bottom-up and top-down uncertainty quantification of bcc Fe plasticity and dislocation-interstitial loop interactions**
Aaron E. Tallman, Zhi Zeng, Cameron Sobie, Yan Wang, Laurent Capolungo, Ting Zhu, and David L. McDowell

Representative Modeling and Simulations Exercised in this Sub-Problem:

Atomistic models for the interaction between interstitial loop and single dislocation in BCC Fe have been developed. The models include a variety of Burgers vectors, habit planes and slip planes.

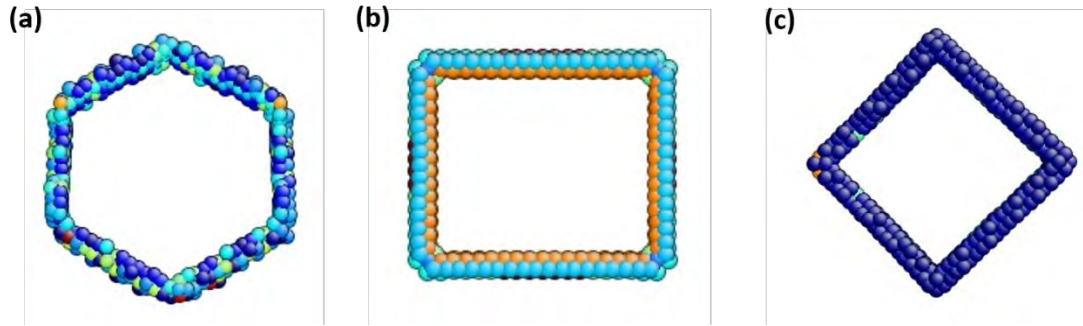


Fig. 2: Atomistic models of interstitial loops in irradiated BCC Fe. (a) Interstitial loop with burgers vector of $\frac{1}{2} \langle 111 \rangle$ and habit plane of $\{110\}$; (b) Interstitial loop with burgers vector of $\frac{1}{2} \langle 100 \rangle$ and habit plane of $\{100\}$; (c) Interstitial loop with burgers vector of $\frac{1}{2} \langle 100 \rangle$ and habit plane of $\{110\}$.

Three typical kinds of interstitial loops that exist in irradiated Fe alloys are recognized and their atomistic models have been built [8-11]. The first kind of the interstitial loops is prismatic dislocation loops with burgers vector of $\frac{1}{2} \langle 111 \rangle$ and habit plane of $\{110\}$, as shown in Fig. 1a. These $\langle 111 \rangle \{110\}$ loops have hexagonal shapes. They are highly mobile so they can easily be passed by a dislocation. The second kind of the interstitial loops is prismatic dislocation loops with Burgers vector of $\frac{1}{2} \langle 100 \rangle$ and habit plane of $\{100\}$, as shown in Fig. 2b. These $\langle 100 \rangle \{100\}$ loops have rectangle shapes with each edges lying on $\{100\}$ direction. They are also glissile. The third kind of the interstitial loops is prismatic dislocation loops with burgers vector of $\frac{1}{2} \langle 100 \rangle$ and habit plane of $\{110\}$, as shown in Fig. 2c. These $\langle 100 \rangle \{110\}$ loops have rhombic shapes. They are sessile.

In order to study the dynamics of a dislocation in association with an SIA loop, a model was developed which includes an edge dislocations was and an $\frac{1}{2} \langle 111 \rangle \{110\}$ dislocation loop. The x, y and z axes of the simulated crystal were oriented along $[111]$, $[\bar{1}\bar{1}2]$ and $[1\bar{1}0]$ directions, as shown in Fig. 3.

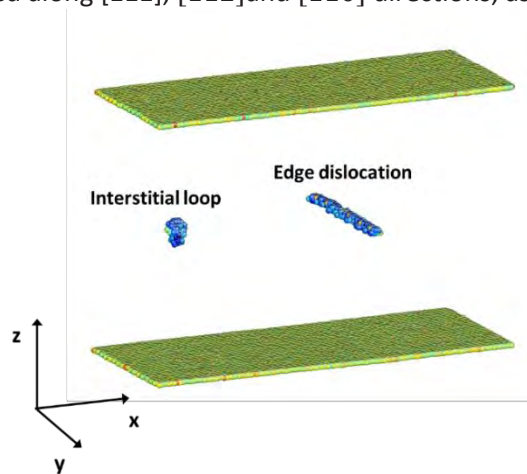


Fig. 3. Atomistic model of dislocation interstitial loop interaction.

Periodic boundary conditions were employed in the x and y directions, corresponding to the direction of **b** and the line direction, respectively, and fixed conditions were used across the z boundaries. The interstitial loop contains 37 SIAs. The dimensions of the simulation structure are $L_x = 29.79\text{nm}$, $L_y = 11.23\text{ nm}$ and $L_z = 30.4\text{ nm}$. The total number of atoms are 573637. Molecular dynamics simulations are performed by LAMMPS. The temperature is maintained at 300K. Three interatomic potentials are used.

They are Finnis–Sinclair-type interatomic potential for Fe of Ackland et al. [12], Finnis-Sinclair-type interatomic potential for Fe of Mendeleev et al. [13] and an EAM potential recently developed by Proville et al. [14]. This facilitates consideration of model form uncertainty in addition to the other geometric factors associated with dislocation-loop interactions.

In pursuing the consideration of uncertainty in Interstitial Loop/Dislocation Interactions in Irradiated Fe Alloys, we employ both a “black box” model based on prior derived hardening laws and results of atomistic simulations.

d) Black box model

Material point simulation of Crystal Plasticity Model (Friedel Kroupa Hirsch hardening with separate treatment for loop types)

e) Bottom-up information (parameter scale data)

Atomistic simulation of interstitial loop – dislocation interactions (Zhi Zeng)

A comprehensive sensitivity study of dislocation interactions with interstitial loops in irradiated BCC Fe was conducted using molecular dynamics simulations. This study focused on interaction of a $\frac{1}{2}\langle 111 \rangle$ {110} edge dislocation with three typical kinds of prismatic interstitial loops:

- $\frac{1}{2}\langle 111 \rangle$ in habit plane of {110}
- $\frac{1}{2}\langle 100 \rangle$ in habit plane of {100}
- $\frac{1}{2}\langle 100 \rangle$ in habit plane of {110}

Furthermore, this study covered a variety kinds of the possibilities of edge dislocation encountering interstitial loops. The results are discussed below. (include the mechanism of interaction categories defined per each data point)

In molecular dynamics simulations, the Burgers vector of the edge dislocation is $\frac{1}{2}\langle 111 \rangle$ and the slip plane is $(\bar{1}10)$. Molecular dynamics simulations compute the critical resolved shear stress necessary to drive an edge dislocation past an interstitial loop. Three typical kinds of interstitial loops is studied. For each kind, there are different scenarios. The critical resolved shear stress is obtained for every scenario.

The comprehensive lists of critical resolved shear stresses give the interstitial loop barrier strength as a multi-dimensional function of parameters.

1. Interstitial loop with Burgers vector of $\frac{1}{2}\langle 111 \rangle$ in habit plane of {110}

Nine interstitial loops of this kind were identified for interaction with dislocation. These interstitial loops have different Burgers vectors and habit planes. These nine loops were identified by considering the misorientation between the Burgers vector of edge dislocation and the Burgers vector of the interstitial loop, the angle between habit plane and Burgers vector of edge dislocation, the angle between the slip plane and the Burgers vector of interstitial loop, and the angle between the slip plane and habit plane. Each loop has three different sizes, corresponding to: 37 SIAs, 99 SIAs and 331 SIAs. They were of hexagonal shape with sides of length: 0.82 nm, 1.34 nm and 2.45 nm, respectively. For each interaction event, simulations were conducted at three temperatures: 100K, 300K and 450K. For each simulation, three interatomic potential are used. The critical resolved shear stress for each case is listed below.

Table 1 Critical resolved shear stress to pass $\frac{1}{2} \langle 111 \rangle \{110\}$ type of interstitial loop

$\frac{1}{2} [11\bar{1}](110)$ Interstitial loop									
	Ackland			Mendelev			Proville		
	37 SIAs	99 SIAs	331 SIAs	37 SIAs	99 SIAs	331 SIAs	37 SIAs	99 SIAs	331 SIAs
100K	25 MPa	90 MPa	270 MPa	34 MPa	96 MPa	279 MPa	36 MPa	108 MPa	289 MPa
300K	12 MPa	63 MPa	220 MPa	20 MPa	72 MPa	225 MPa	31 MPa	75 MPa	234 MPa
450K	0 MPa	26 MPa	160 MPa	0 MPa	27 MPa	162 MPa	0 MPa	45 MPa	171 MPa

$\frac{1}{2} [11\bar{1}](\bar{1}10)$ Interstitial loop									
	Ackland			Mendelev			Proville		
	37 SIAs	99 SIAs	331 SIAs	37 SIAs	99 SIAs	331 SIAs	37 SIAs	99 SIAs	331 SIAs
100K	26 MPa	130 MPa	290 MPa	93 MPa	89 MPa	275 MPa	45 MPa	110 MPa	294 MPa
300K	19 MPa	97 MPa	250 MPa	20 MPa	83 MPa	223 MPa	23 MPa	80 MPa	236 MPa
450K	15 MPa	77 MPa	170 MPa	14 MPa	80 MPa	158 MPa	16 MPa	48 MPa	178 MPa

$\frac{1}{2} [111](110)$ Interstitial loop									
	Ackland			Mendelev			Proville		
	37 SIAs	99 SIAs	331 SIAs	37 SIAs	99 SIAs	331 SIAs	37 SIAs	99 SIAs	331 SIAs
100K	0 MPa	0 MPa	0 MPa	0 MPa	0 MPa	0 MPa	0 MPa	0 MPa	0 MPa
300K	0 MPa	0 MPa	0 MPa	0 MPa	0 MPa	0 MPa	0 MPa	0 MPa	0 MPa
450K	0 MPa	0 MPa	0 MPa	0 MPa	0 MPa	0 MPa	0 MPa	0 MPa	0 MPa

$\frac{1}{2} [111](\bar{1}10)$ Interstitial loop									
	Ackland			Mendelev			Proville		
	37 SIAs	99 SIAs	331 SIAs	37 SIAs	99 SIAs	331 SIAs	37 SIAs	99 SIAs	331 SIAs
100K	0 MPa	0 MPa	0 MPa	0 MPa	0 MPa	0 MPa	0 MPa	0 MPa	0 MPa
300K	0 MPa	0 MPa	0 MPa	0 MPa	0 MPa	0 MPa	0 MPa	0 MPa	0 MPa
450K	0 MPa	0 MPa	0 MPa	0 MPa	0 MPa	0 MPa	0 MPa	0 MPa	0 MPa

$\frac{1}{2} [1\bar{1}1](110)$ Interstitial loop									
	Ackland			Mendelev			Proville		
	37 SIAs	99 SIAs	331 SIAs	37 SIAs	99 SIAs	331 SIAs	37 SIAs	99 SIAs	331 SIAs
100K	87 MPa	180 MPa	270 MPa	91 MPa	177 MPa	268 MPa	96 MPa	182 MPa	273 MPa
300K	48 MPa	149 MPa	238 MPa	51 MPa	146 MPa	241 MPa	50 MPa	150 MPa	242 MPa
450K	16 MPa	123 MPa	188 MPa	17 MPa	123 MPa	186 MPa	24 MPa	126 MPa	194 MPa

$\frac{1}{2} [1\bar{1}1](\bar{1}10)$ Interstitial loop									
	Ackland			Mendelev			Proville		
	37 SIAs	99 SIAs	331 SIAs	37 SIAs	99 SIAs	331 SIAs	37 SIAs	99 SIAs	331 SIAs
100K	86 MPa	214 MPa	285 MPa	86 MPa	216 MPa	285 MPa	91 MPa	215 MPa	285 MPa
300K	62 MPa	169 MPa	269 MPa	62 MPa	167 MPa	268 MPa	62 MPa	178 MPa	273 MPa
450K	14 MPa	135 MPa	255 MPa	17 MPa	139 MPa	257 MPa	15 MPa	142 MPa	260 MPa

$\frac{1}{2} [111](\bar{1}01)$ Interstitial loop									
	Ackland			Mendelev			Proville		
	37 SIAs	99 SIAs	331 SIAs	37 SIAs	99 SIAs	331 SIAs	37 SIAs	99 SIAs	331 SIAs
100K	36 MPa	157 MPa	288 MPa	38 MPa	154 MPa	289 MPa	40 MPa	166 MPa	293 MPa
300K	22 MPa	87 MPa	247 MPa	19 MPa	87 MPa	245 MPa	29 MPa	89 MPa	255 MPa
450K	12 MPa	70 MPa	202 MPa	11 MPa	69 MPa	203 MPa	18 MPa	70 MPa	203 MPa

$\frac{1}{2} [11\bar{1}](\bar{1}01)$ Interstitial loop									
	Ackland			Mendelev			Proville		
	37 SIAs	99 SIAs	331 SIAs	37 SIAs	99 SIAs	331 SIAs	37 SIAs	99 SIAs	331 SIAs
100K	81 MPa	217 MPa	276 MPa	81 MPa	213 MPa	279 MPa	83 MPa	226 MPa	277 MPa
300K	47 MPa	192 MPa	265 MPa	43 MPa	196 MPa	268 MPa	50 MPa	196 MPa	267 MPa
450K	22 MPa	114 MPa	244 MPa	26 MPa	111 MPa	246 MPa	22 MPa	122 MPa	245 MPa

$\frac{1}{2} [\bar{1}\bar{1}\bar{1}](\bar{1}01)$ Interstitial loop									
	Ackland			Mendelev			Proville		
	37 SIAs	99 SIAs	331 SIAs	37 SIAs	99 SIAs	331 SIAs	37 SIAs	99 SIAs	331 SIAs
100K	75 MPa	157 MPa	288 MPa	75 MPa	160 MPa	288 MPa	75 MPa	159 MPa	297 MPa
300K	44 MPa	141 MPa	261 MPa	47 MPa	138 MPa	260 MPa	44 MPa	142 MPa	261 MPa
450K	8 MPa	112 MPa	198 MPa	5 MPa	112 MPa	199 MPa	12 MPa	112 MPa	203 MPa

2. Interstitial loop with Burgers vector of $\langle 100 \rangle$ in habit plane of $\{110\}$

Nine interstitial loops of this kind were identified for interaction with dislocations. Each loop corresponds to three different sizes: 30 SIAs, 169 SIAs and 331 SIAs. They were of rhombic shape with sides of length: 1.09 nm, 2.6 nm and 3.6 nm, respectively. For each interaction event, simulations were conducted in three temperatures: 100K, 300K and 450K. The critical resolved shear stress for each case is listed below:

Table 2 Critical resolved shear stress to pass $\langle 100 \rangle \{110\}$ type of interstitial loop

$[100](110)$ Interstitial loop									
	Ackland			Mendelev			Proville		
	30 SIAs	169 SIAs	331 SIAs	30 SIAs	169 SIAs	331 SIAs	30 SIAs	169 SIAs	331 SIAs
100K	67 MPa	219 MPa	312 MPa	67 MPa	218 MPa	311 MPa	67 MPa	228 MPa	314 MPa
300K	47 MPa	200 MPa	299 MPa	47 MPa	204 MPa	301 MPa	51 MPa	209 MPa	299 MPa
450K	27 MPa	92 MPa	239 MPa	31 MPa	91 MPa	236 MPa	29 MPa	93 MPa	244 MPa

$[010](011)$ Interstitial loop									
	Ackland			Mendelev			Proville		
	30 SIAs	169 SIAs	331 SIAs	30 SIAs	169 SIAs	331 SIAs	30 SIAs	169 SIAs	331 SIAs
100K	74 MPa	177 MPa	293 MPa	78 MPa	178 MPa	293 MPa	81 MPa	178 MPa	300 MPa
300K	55 MPa	130 MPa	257 MPa	58 MPa	127 MPa	258 MPa	57 MPa	136 MPa	263 MPa
450K	25 MPa	104 MPa	224 MPa	24 MPa	100 MPa	226 MPa	30 MPa	105 MPa	227 MPa

$[001](\bar{1}01)$ Interstitial loop									
	Ackland			Mendelev			Proville		
	30 SIAs	169 SIAs	331 SIAs	30 SIAs	169 SIAs	331 SIAs	30 SIAs	169 SIAs	331 SIAs
100K	46 MPa	113 MPa	182 MPa	48 MPa	113 MPa	182 MPa	52 MPa	118 MPa	190 MPa
300K	33 MPa	100 MPa	135 MPa	37 MPa	100 MPa	135 MPa	40 MPa	108 MPa	144 MPa
450K	21 MPa	60 MPa	105 MPa	17 MPa	60 MPa	103 MPa	29 MPa	63 MPa	108 MPa

[100](011) Interstitial loop									
	Ackland			Mendelev			Proville		
	30 SIAs	169 SIAs	331 SIAs	30 SIAs	169 SIAs	331 SIAs	30 SIAs	169 SIAs	331 SIAs
100K	70 MPa	168 MPa	227 MPa	70 MPa	168 MPa	224 MPa	72 MPa	177 MPa	236 MPa
300K	27 MPa	120 MPa	219 MPa	28 MPa	119 MPa	222 MPa	28 MPa	123 MPa	220 MPa
450K	11 MPa	95 MPa	196 MPa	11 MPa	93 MPa	194 MPa	13 MPa	99 MPa	200 MPa

[010](110) Interstitial loop									
	Ackland			Mendelev			Proville		
	30 SIAs	169 SIAs	331 SIAs	30 SIAs	169 SIAs	331 SIAs	30 SIAs	169 SIAs	331 SIAs
100K	69 MPa	198 MPa	302 MPa	66 MPa	199 MPa	304 MPa	71 MPa	203 MPa	310 MPa
300K	46 MPa	99 MPa	261 MPa	46 MPa	98 MPa	260 MPa	47 MPa	103 MPa	263 MPa
450K	21 MPa	86 MPa	214 MPa	25 MPa	84 MPa	212 MPa	23 MPa	89 MPa	214 MPa

[001](101) Interstitial loop									
	Ackland			Mendelev			Proville		
	30 SIAs	169 SIAs	331 SIAs	30 SIAs	169 SIAs	331 SIAs	30 SIAs	169 SIAs	331 SIAs
100K	55 MPa	204 MPa	326 MPa	57 MPa	202 MPa	326 MPa	59 MPa	207 MPa	326 MPa
300K	26 MPa	170 MPa	299 MPa	30 MPa	170 MPa	303 MPa	28 MPa	176 MPa	308 MPa
450K	16 MPa	77 MPa	247 MPa	12 MPa	77 MPa	247 MPa	21 MPa	83 MPa	250 MPa

[100](101) Interstitial loop									
	Ackland			Mendelev			Proville		
	30 SIAs	169 SIAs	331 SIAs	30 SIAs	169 SIAs	331 SIAs	30 SIAs	169 SIAs	331 SIAs
100K	31 MPa	67 MPa	97 MPa	33 MPa	66 MPa	99 MPa	35 MPa	76 MPa	103 MPa
300K	23 MPa	50 MPa	82 MPa	27 MPa	48 MPa	78 MPa	29 MPa	57 MPa	85 MPa
450K	8 MPa	39 MPa	72 MPa	11 MPa	35 MPa	73 MPa	9 MPa	46 MPa	80 MPa

[010](101) Interstitial loop									
	Ackland			Mendelev			Proville		
	30 SIAs	169 SIAs	331 SIAs	30 SIAs	169 SIAs	331 SIAs	30 SIAs	169 SIAs	331 SIAs
100K	32 MPa	63 MPa	98 MPa	34 MPa	67 MPa	102 MPa	33 MPa	63 MPa	107 MPa
300K	18 MPa	50 MPa	85 MPa	14 MPa	50 MPa	86 MPa	23 MPa	58 MPa	86 MPa
450K	9 MPa	35 MPa	76 MPa	6 MPa	35 MPa	77 MPa	17 MPa	37 MPa	80 MPa

[001](110) Interstitial loop									
	Ackland			Mendelev			Proville		
	30 SIAs	169 SIAs	331 SIAs	30 SIAs	169 SIAs	331 SIAs	30 SIAs	169 SIAs	331 SIAs
100K	65 MPa	239 MPa	377 MPa	65 MPa	235 MPa	373 MPa	73 MPa	244 MPa	385 MPa
300K	36 MPa	190 MPa	352 MPa	36 MPa	191 MPa	352 MPa	44 MPa	196 MPa	358 MPa
450K	24 MPa	157 MPa	313 MPa	26 MPa	153 MPa	309 MPa	32 MPa	158 MPa	322 MPa

3. Interstitial loop with Burgers vector of $\langle 100 \rangle$ in habit plane of $\{100\}$

Six interstitial loops of this kind were identified for interactions with dislocation. Each loop has three different sizes: 30 SIAs, 169 SIAs and 331 SIAs. They were of square shape with sides of length: 1.09 nm, 2.6 nm and 3.6 nm, respectively. For each interaction event, simulations were conducted in three temperatures: 100K, 300K and 450K. The critical resolved shear stress for each case is listed below.

Table 3 Critical resolved shear stress to pass $\langle 100 \rangle \{100\}$ type of interstitial loop

[001](100) Interstitial loop									
	Ackland			Mendelev			Proville		
	30 SIAs	169 SIAs	331 SIAs	30 SIAs	169 SIAs	331 SIAs	30 SIAs	169 SIAs	331 SIAs
100K	112 MPa	264 MPa	379 MPa	115 MPa	261 MPa	382 MPa	117 MPa	270 MPa	379 MPa
300K	91 MPa	221 MPa	328 MPa	91 MPa	218 MPa	331 MPa	94 MPa	227 MPa	332 MPa
450K	44 MPa	178 MPa	283 MPa	44 MPa	174 MPa	282 MPa	44 MPa	182 MPa	284 MPa

010 Interstitial loop									
	Ackland			Mendelev			Proville		
	30 SIAs	169 SIAs	331 SIAs	30 SIAs	169 SIAs	331 SIAs	30 SIAs	169 SIAs	331 SIAs
100K	134 MPa	283 MPa	383 MPa	131 MPa	280 MPa	387 MPa	136 MPa	292 MPa	386 MPa
300K	58 MPa	241 MPa	353 MPa	55 MPa	238 MPa	357 MPa	65 MPa	246 MPa	362 MPa
450K	25 MPa	181 MPa	316 MPa	29 MPa	180 MPa	315 MPa	25 MPa	186 MPa	320 MPa

001 Interstitial loop									
	Ackland			Mendelev			Proville		
	30 SIAs	169 SIAs	331 SIAs	30 SIAs	169 SIAs	331 SIAs	30 SIAs	169 SIAs	331 SIAs
100K	97 MPa	257 MPa	367 MPa	97 MPa	254 MPa	364 MPa	105 MPa	260 MPa	368 MPa
300K	63 MPa	225 MPa	332 MPa	64 MPa	226 MPa	336 MPa	68 MPa	226 MPa	341 MPa
450K	38 MPa	131 MPa	291 MPa	40 MPa	131 MPa	288 MPa	38 MPa	137 MPa	295 MPa

[010](100) Interstitial loop									
	Ackland			Mendelev			Proville		
	30 SIAs	169 SIAs	331 SIAs	30 SIAs	169 SIAs	331 SIAs	30 SIAs	169 SIAs	331 SIAs
100K	128 MPa	262 MPa	364 MPa	127 MPa	262 MPa	362 MPa	130 MPa	264 MPa	371 MPa
300K	70 MPa	235 MPa	350 MPa	71 MPa	235 MPa	350 MPa	75 MPa	241 MPa	359 MPa
450K	27 MPa	200 MPa	291 MPa	30 MPa	197 MPa	288 MPa	30 MPa	199 MPa	299 MPa

[001](010) Interstitial loop									
	Ackland			Mendelev			Proville		
	30 SIAs	169 SIAs	331 SIAs	30 SIAs	169 SIAs	331 SIAs	30 SIAs	169 SIAs	331 SIAs
100K	108 MPa	192 MPa	387 MPa	105 MPa	195 MPa	383 MPa	109 MPa	192 MPa	393 MPa
300K	62 MPa	155 MPa	341 MPa	62 MPa	158 MPa	341 MPa	65 MPa	159 MPa	345 MPa
450K	27 MPa	142 MPa	278 MPa	26 MPa	146 MPa	276 MPa	31 MPa	143 MPa	283 MPa

[010](001) Interstitial loop									
	Ackland			Mendelev			Proville		
	30 SIAs	169 SIAs	331 SIAs	30 SIAs	169 SIAs	331 SIAs	30 SIAs	169 SIAs	331 SIAs
100K	137 MPa	254 MPa	375 MPa	133 MPa	254 MPa	378 MPa	182 MPa	260 MPa	375 MPa
300K	81 MPa	217 MPa	335 MPa	82 MPa	216 MPa	335 MPa	90 MPa	218 MPa	339 MPa
450K	25 MPa	178 MPa	286 MPa	26 MPa	174 MPa	287 MPa	32 MPa	181 MPa	293 MPa

f) Top-down information (output scale data)

Propagation of uncertainty from multiple options for interatomic potential will be measured by formulating a model that can accept the MD findings into constitutive equations, including the potential for multiple mechanisms for interactions based on loop sizes. This linkage needs to be consistent in assumption and form for all three interatomic potentials' results, so as to allow for the model form to remain constant, while still being able to calibrate to differences in the estimated mechanistic transition size of loops. The top-down continuum model is a dispersed barrier hardening model employed at the slip system level.

Sub-problem 2: Void Nucleation, Growth and Interactions with Dislocations in Irradiated Fe Alloys

Students: Richard Hoffman Alex Moore, and Aaron Tallman

Faculty: Chaitanya Deo and David McDowell

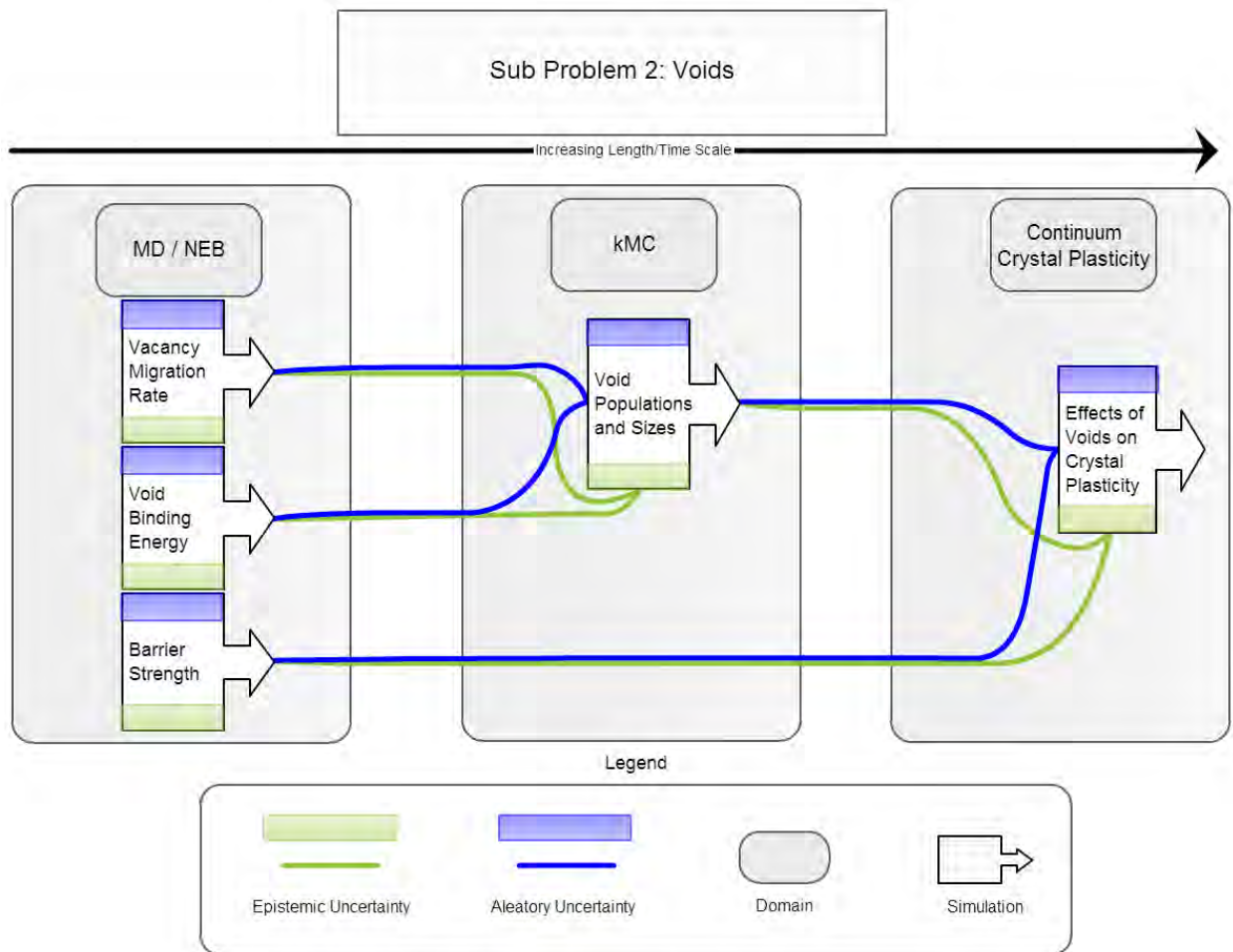
Void growth in irradiated materials is an important factor in determination of deformation mechanics. While alloy choices can largely mitigate the size and number of voids in an irradiated bcc iron alloy, some voids remain. The treatment of these obstacles may present a source of variance in the predictions of a

multiscale model. Investigation has been planned and is underway concerning the inclusion of voids in the modeling of bcc iron alloys. A configuration of this sub-problem appears in the chart below.

Simulation models for the second sub-problem are defined as follows:

1. MD/NEB simulation of the binding energy of voids
2. MD/NEB simulation of voids to inform the migration rate of vacancies
3. NEB simulation of void-dislocation interactions to determine the barrier strength of voids to dislocation glide
4. KMC simulation of void formation to inform values for void populations and size distributions
5. Incorporation of these data in a constitutive relation between void population and deformation in the continuum model

Bcc Fe irradiated at various temperatures has been found to contain voids. A current multiscale model of this material has not incorporated void nucleation into the analysis of its crystal plasticity. Voids and micro voids have significant effects on the deformation of metal crystals. The incorporation of void nucleation into a model of crystal plasticity is a necessary step in the development of a fully comprehensive analysis of the material. It also presents an opportunity to call upon lower length scale simulations to inform the CCP model's treatment of unit processes.



The KMC modeling used to inform crystal plasticity modeling addresses both KMC and Crystal Plasticity uncertainty sources and representation in Task 1. Professor C. Deo's work has focused on addressing uncertainty in Kinetic Monte Carlo (KMC) methods, including dependence on rate catalog models. This work has compared different inputs to KMC simulations in order to determine how changes in the rate catalog may affect accuracy and results.

Several journal articles are planned as an outcome of this sub-problem:

- **Sensitivity analysis of Point Defect Balance Equations**
Trey Hoffman, Aaron Tallman, Chaitanya Deo, David McDowell
- **Structural Uncertainty Quantification in Rate Law simulation of bcc metal irradiation-void nucleation and growth**
Trey Hoffman, Aaron Tallman, Alex Moore, Chaitanya Deo, David L. McDowell
- **Rate Law simulation of bcc Fe irradiation-void nucleation and growth, with Uncertainty Propagation through Crystal Plasticity modeling of irradiated bcc Fe**
Aaron Tallman, Trey Hoffman, Alex Moore, Yan Wang, Chaitanya Deo, David L. McDowell

Representative Modeling and Simulations Exercised in this Sub-Problem:

Sensitivity analysis of Kinetic Monte Carlo simulations of diffusivity – A defect diffusion model under radiation damage has been developed and is being validated. Point defect balance equations are simulated. The time evolution of the number densities of the interstitials $n_i(t)$ and vacancies $n_v(t)$ is given by the coupled nonlinear equations

$$\begin{aligned} \frac{dn_i}{dt} &= \sigma F - K_v \omega_{v_i} n_i - K_i \omega_{v_i} n_v - K_{is} \omega_s n_i \\ \frac{dn_v}{dt} &= \sigma F - K_v \omega_{v_i} n_i - K_i \omega_{v_i} n_v - K_{vs} \omega_s n_v \end{aligned} \quad (1)$$

The mixed encounter rate ω_{iD} counter rate ω_{vD} , but is reduced ratio of the number of rotation rate has also been derived in the kinetics in the intermediate

where the first term on right is the production term and each negative term on right is a loss term for the sinks. These relations may be interpreted according to

$$\text{rate of defects} = \text{production rate} - \text{recombination rate} - \text{sink annihilation rate}$$

We employ SPPARKS with defect production, recombination and annihilation rates to get point defect balance evolution over multiple length and time scales.

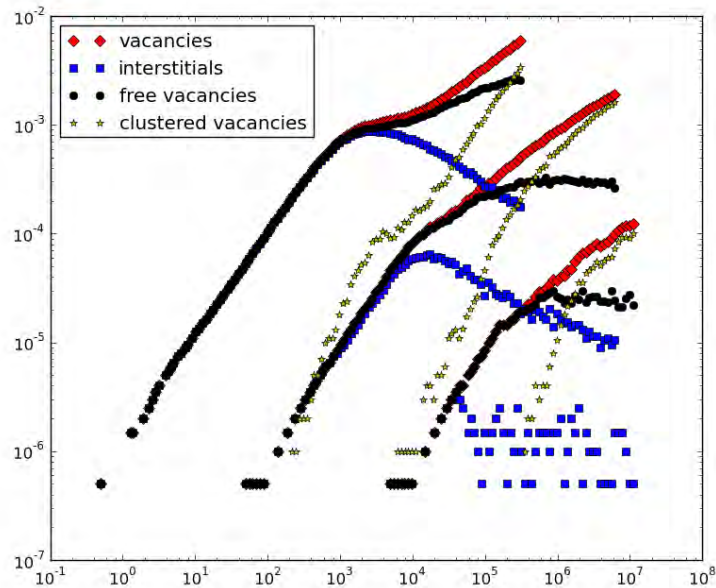


Fig. 4. Results of simulations where the point defect balance is shown, allowing immobile vacancy clusters to form.

2. *Incorporation of void nucleation information in crystal plasticity framework* – Void nucleation has been simulated with KMC calculations. Parameters from MD that go into the void nucleation rate will be identified and these will then be used to calculate void nucleation in bcc Fe. This information will be upscaled to the Crystal Plasticity framework. Epistemic and Aleatory uncertainties will be identified in the MD and the rate theory/KMC codes.

3. *Uncertainty quantification of calculations of void energetics with different interatomic potentials (EAM, MEAM)* - Two interatomic potentials (EAM and MEAM) have been used to calculate the formation energy of voids of various sizes at various temperatures. The differences between the two potentials will be identified and the aleatory and epistemic uncertainties is being identified.

As materials modeling efforts begin to incorporate multiple models in the analysis of a single material, Uncertainty Quantification, or UQ, is becoming a powerful tool in coordinating the information exchanged between these models. The multi-scale modeling of voids in irradiated bcc Fe presents an opportunity to demonstrate uses of UQ. Top-Down and Bottom-Up model form UQ is performed on the kMC simulation of void nucleation and growth in irradiated bcc Fe. These UQ results are used for a study of uncertainty propagation in a continuum Crystal Plasticity model.

The KMC code is a modification of the diffusion model contained in SPPARKS{citation for SPPARKS}. The chance of an event occurring is based on an Arrhenius type probability: $R = \exp(-E/kT)$.

The code is modified to allow for the treatment of different defect types separately. Modifications were also made to account for the irradiation process. At prescribed times based on the irradiation rate. In addition sinks can be modeled in one of two ways: as physical objects interspersed on the lattice or a statistical probability of defect elimination based on the given sink concentration. Early analysis suggests

these two methods are equivalent and thus the simpler statistical approach is generally chosen. Each of the types of defects involved in the simulation is treated differently. In the discussion of defects below a collision refers to the result of a defect jumping to a lattice site next to another defect

Vacancies are the simplest of defects to treat in the KMC model they move in three dimensions through a series of diffusive jumps, each of which is controlled by a single energy barrier, E_{VM} . They can be removed from the simulation in one of three ways: collision with an interstitial resulting in elimination of the pair, statistical elimination to simulate contact with a sink, and a collision with an n sized void thus forming a part of an $n + 1$ sized void. The vacancies can be formed through three distinct processes: irradiation induced pair creation, separation from an n sized void resulting in an $n-1$ sized void and a single vacancy, and interstitial collision with a void of size 2 resulting in a single vacancy remaining.

In this model voids are treated a group of vacancies that may leave the void by overcoming a barrier if there is an available neighboring site. The barrier for leaving the void is found through atomistic simulations and varies based on the size of the void, $E(x)_V + E_{VM}$. Thus the members and size of a void must be followed throughout the simulation resulting in the majority of the added computational complexity of the simulation. Voids are created and grow as a result of vacancies colliding with a vacancy or a void respectively. They are reduced in size or destroyed through the above process of vacancies leaving the void and from collision of interstitials with the void.

Interstitials simulation is composed of two parts. In order to approximate the 1D motion of interstitials through the crystal, interstitials have two types of motion. The first is a diffusive jump in the chosen 111 direction and the second is a rotation into another 111 direction. Each of these jumps types is given an energy associated with it: E_{IM} and E_R , respectively. We consider parametrically the role of

- Diffusivity of interstitials
- Diffusivity of vacancies
- Binding energy of voids

Atomistic simulations of iron voids will be able to obtain some of the base energetic properties of voids, which are not directly or easily obtainable using experimental methods. The energetics of the simulated void system can be coupled with larger scale simulations in order to bridge the simulation gap from the atomistic scale to the continuum scale.

The molecular statics/dynamics energetics of the iron voids are not enough to fully couple the atomistic and the crystal plasticity simulations. While voids can be added to the defect rate balance equations found in crystal plasticity, typically sink strengths may be required. The issue lies in the fact that the sink strength is not directly obtainable from the void energetics, but would require an elastic field study on the local point defects. However, it may be possible for the energetics to be incorporated via vacancy emission efficiency as seen in Woo and Singh in 1992 (Woo, C. H., and B. N. Singh. "Production bias due to clustering of point defects in irradiation-induced cascades." *Philosophical Magazine A* 65.4 (1992): 889-912), if additional assumptions are made.

However the vacancy formation energy does play a direct role in determining the diffusivity of vacancies and thus the efficiency with which point defects are captured at sinks or mutually annihilate.

Further investigated was the influence of interatomic potentials on the formation energy of vacancies and vacancy clusters. Molecular dynamics simulations were conducted with four different interatomic potentials as shown in Table 4.

Table 4: Semi-empirical Fe Potentials

Potential #	Who Developed	Type	Why Developed
1	Mendelev et al. 2003 (1)	EAM	Developed for both crystalline and liquid Fe
2	Lee et al. 2001 (2)	MEAM-0	Developed to mimic 0K elastic constants and formation energies of Fe at 0K
3	Lee et al. 2012 (3)	MEAM-T	Developed to mimic correct structural phase behavior of Fe with respect to temperature
4	Lee et al. 2012 (3)	MEAM-P	Developed to mimic correct structural phase behavior of Fe with respect to pressure

In each case, In order to estimate the void stability and formation energy, a periodic super-cell consisting of 10x10x10 body centered cubic (BCC) unit-cells (2000 atoms in the defect free system) was simulated. We performed energy minimization in order to achieve the energy of a perfect BCC lattice.

Then in order to calculate the defect formation energy of a vacancy, an atom was removed from the perfect bcc lattice creating a vacancy in the system. This new system with the vacancy then underwent another energy minimization to find the relaxed structure. Then the vacancy formation energy can be calculated using these relaxed structure energies:

$$E_{f,vac} = E_{(n-1)} - \frac{n-1}{n} E_n$$

The formation energy of a void can be calculated similar to that of a vacancy, but now you have multiple clustered vacancies creating a void. The formation energy of a void can be calculated by:

$$E_{f,void}(x) = E_{(n-x)} - \frac{n-x}{n} E_n$$

where x is the number of vacancies in the void.

The formation energies can then be used to find the vacancy binding energy to an existing void. The binding energy can be obtained by

$$BE_{vac}(x) = E_{f,void}(x-1) + E_{f,vac} - E_{f,void}(x)$$

where x is the size of the existing void. This binding energy of the vacancy to a void can be directly incorporated into the larger scale kinetic monte-carlo (KMC) simulations.

In addition, the volumetric swelling percentage can also be calculated using the equation

$$\frac{\Delta V}{V_0} = \frac{(V_{system} + n_{vac}V_{atom}) - V_0}{V_0}$$

where V_{system} is total volume of system with a void, n_{vac} is number of vacancies that constitute the void, V_{atom} is the volume per atom in a defect free system, and V_0 is the volume of pure system.

We can use the relationship $\Delta V/V = 4/3\pi R^3\rho_v$ to determine the amount of swelling, where R is the average void size and ρ_v is the void density. We can get both of these values from a completed KMC simulation. Using these potentials, we can see the influence of model form on vacancy formation and migration energies (Table 5), as well as void formation energy (Fig. 5) and vacancy binding energies.

Table 5: Vacancy Formation Energy and Vacancy Migration Energy Comparison

Property	Experimental	DFT	MEAM-P	MEAM-T
Vacancy Formation Energy	1.53, 2.0	1.95, 2.18	1.65	1.6
Vacancy Migration Energy	0.55	0.65	0.14	0.22

Both the MEAM-P and MEAM-T potentials perform most unsatisfactorily for self-diffusion, significantly underestimating their vacancy migration energies, which are respectively only about 20% and 40% of the experimental value.

Figure 5 shows the void formation energy for the three potentials namely the EAM, MEAM-T and the MEAM-P. The formation energy difference between the three potentials can be seen in the figure above. The MEAM-0 potential was found to be unstable after the introduction of defects and could not be used. The epistemic uncertainty from the differing semi-empirical potential used in a 35 vacancy void is seen to be as large as approximately 10 eV. Each semi-empirical potential formation energy versus number of vacancies in the void was fit to a power law equation. The power law fit has been used by previous simulations and been shown to work reasonably well.

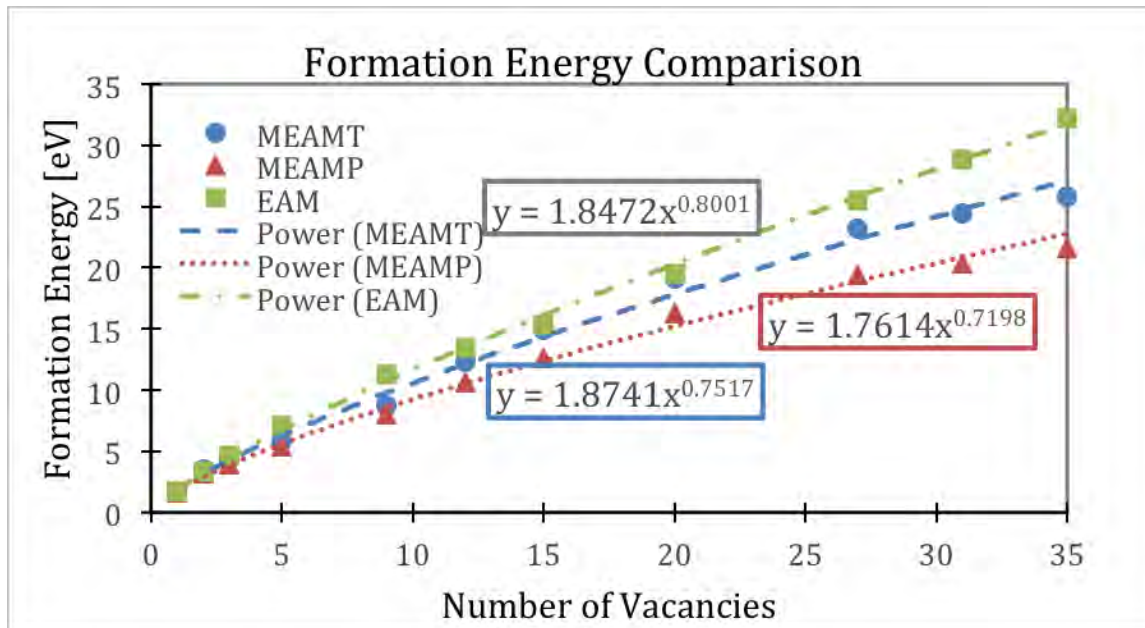


Fig. 5: Power law fit of the Void Formation Energy for the EAM, MEAM-T, and MEAM-P Potentials.

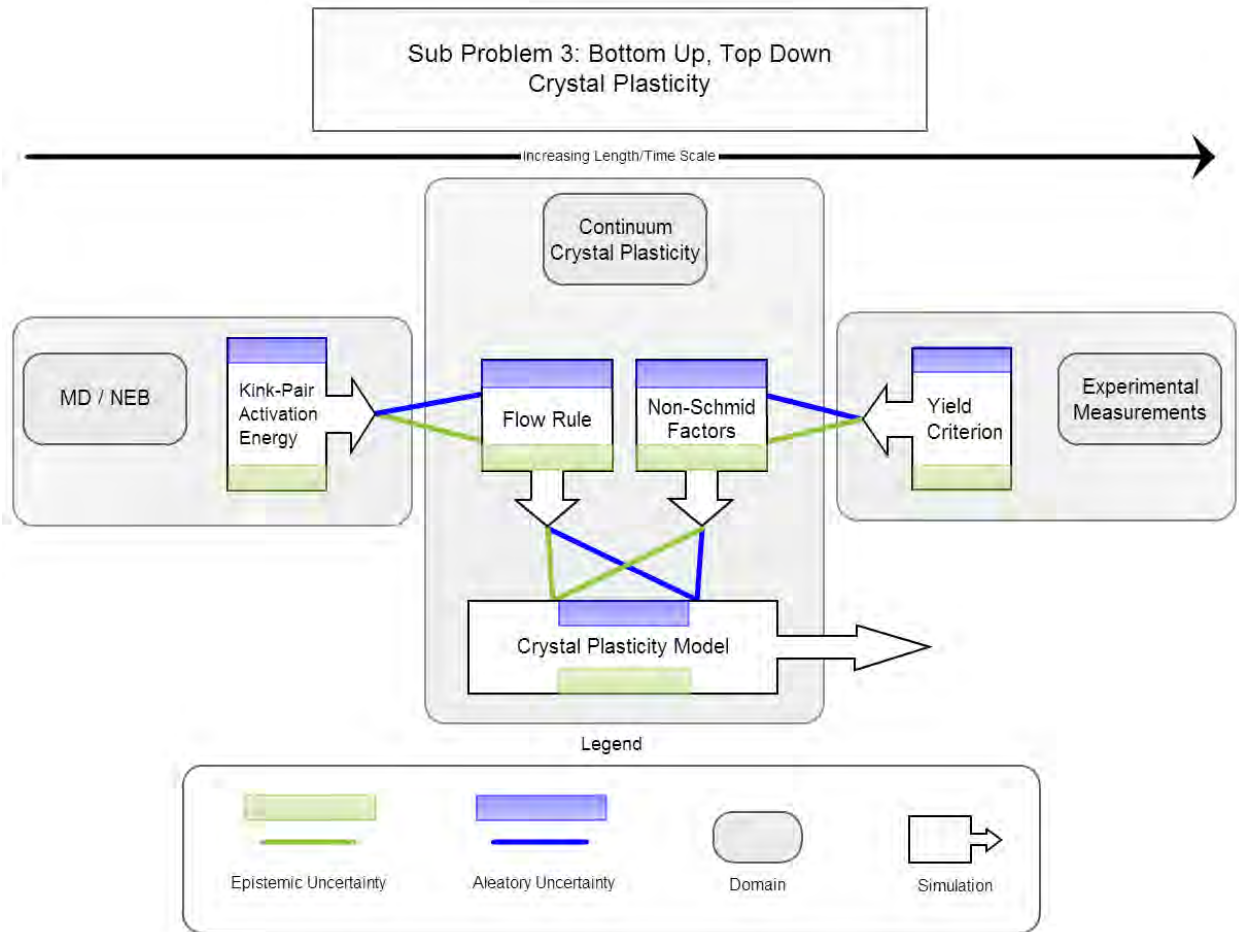
Sub-problem 3: Bottom-Up and Top-Down Uncertainty in Informing Crystal Plasticity for BCC Systems

Students: Aaron Tallman

Faculty: Ting Zhu, Yan Wang and David McDowell

While the previous subproblems concern the use of MD and KMC to strengthen the predictions made by the CCP model, this subproblem addresses a case where the information travels both up and down the length scale. This case examines the glide of dislocations, and it uses information from MD to inform the kink-pair nucleation mechanism, and experimental measurements are used to inform the yield criterion used in the flow rule. Within the model framework, this ability to coordinate information from various sources is being pursued. A method for measuring the uncertainty endemic to model form is being developed and applied to a Top-down and Bottom-up Crystal Plasticity model of bcc Fe. Forward and Inverse UQ approaches are used in combination to measure the uncertainty related to the given model's performance in bridging two sources of information across time/length scale domains.

The mechanisms under investigation in this sub-problem are kink-pair nucleation and the non-Schmid behavior related to the initial yield criterion. An initial configuration of this sub-problem appears in the chart below.



Experimental and simulation models for this sub-problem are being pursued as follows:

1. NEB simulation of kink-pair nucleation to inform the estimation of kink-pair activation energy
2. Incorporation of the kink pair activation energy in a flow rule to be used with CCP modeling
3. Experimental measurement of yield criterion in the material in order to inform non-Schmid coefficient values
4. Incorporation of non-Schmid coefficients in CCP model to account for non-Schmid behavior

In BCC metals, the cores of dislocations must be constricted to a single glide plane in order to become glissile. In irradiated materials, the high concentration of interstitials they contain are expected to have an effect on this core constriction. The relation between the interstitial concentration and the effects of core spreading must be identified in atomistic simulations. Atomistic simulations are being pursued regarding finite temperature dislocation core spreading coupled with interstitials (Zhi Zeng and Sankar Narayanan, advised by T. Zhu).

Incorporation of these effects into the yield criteria of crystal plasticity is also being pursued (Aaron Tallman, advised by D.L. McDowell and Y. Wang). We will employ continuum crystal plasticity constitutive equations to relate interstitial concentration to the values of the Non-Schmid coefficients in the slip system level yield relations.

The KMC modeling used to inform crystal plasticity modeling addresses both KMC and Crystal Plasticity uncertainty sources and representation in Task 1. PhD student Trey Hoffmann presented “KMC simulation of diffusion in fluorite lattice” at Multiscale Modeling and Simulation of Nuclear Fuel (MMSNF) in Chicago, IL in October 2013.

Non-Schmid effects on dislocation core constriction were not considered in previous versions of the crystal plasticity model for irradiated Fe-based alloys. Recent atomistic simulations within our team based on an improved interatomic potential have shed light on new understanding of mobility of screw dislocations based on coordinated kink-pair formation (work done by Sankar Narayanan, advised by T. Zhu), which does not rely on the notion of dislocation core spreading. On the other hand, based on top-down fitting single crystal and polycrystal experimental data on laboratory scale specimens as a function of strain rate and temperature, Anirban Patra (advised by D.L. McDowell) has found that even at room temperature, the Non Schmid stresses have appreciable asymmetry effects and a phenomenological core spreading model (following the earlier works of Vitek and Bassani) is a key ingredient. Hence, there is considerable uncertainty regarding the physics (nanoscale or mesoscale) that governs core spreading (non-Schmid) effects on yield of BCC crystals as a function of temperature and how to best use a combined bottom-up and top-down strategy to estimate both model form and model parameters. We have set the stage for this uncertainty sub-problem by conducting comprehensive efforts in using both atomistics-based, bottom-up simulations (Narayanan et al.) and top-down experimental approaches (Patra et al.), as in the following archival journal articles:

- Narayanan, S., McDowell, D.L., and Zhu, T., “Crystal Plasticity Model for BCC Iron Atomistically Informed by Kinetics of Correlated Kinkpair Nucleation on Screw Dislocations,” *Journal of the Mechanics and Physics of Solids*, Vol. 65, 2014, pp. 54-68.
- Patra, A., Zhu, T. and McDowell, D.L., “Constitutive equations for modeling non-Schmid effects in single crystal bcc-Fe at low and ambient temperatures,” *Int. J. Plasticity*, Vol. 59, 2014, pp. 1-14.

Both approaches have been used to establish crystal plasticity models of somewhat different model form and different values of model parameters for the same phenomena. This sub-problem hence provides a potentially very fruitful opportunity for multiscale uncertainty quantification and management. This sub-problem focuses on the crystal plasticity aspect of Task 1 – Uncertainty sources and representation, while also involving aspects of Task 1, MD - Uncertainty sources and representation in models.

Zhi Zeng has pursued unit process Nudged Elastic Band modeling to quantify the effects of point defect, defect cluster, free surface and grain boundary on energy barriers of screw dislocation migration. These data would provide the quantitative atomistic input into the uncertainty sub-problem sensitivity studies in the third year of the program. In addition, we continue to perform the crystal plasticity modeling to study the uncertainty effects of grain size and spatial distribution on the yield strength, strain hardening and ductility.

Task 1. Crystal plasticity – uncertainty sources and representation

Uncertainty sub-problems 1-3 defined in the Task 1- ab initio, MD, KMC sub-task above relate directly to informing crystal plasticity. Sub-problem 3 considers multiscale aspects from both bottom-up and top-down perspectives; a partial listing of the associated uncertainty sources appears below for each class of approach. As a component of the crystal plasticity work, T. Zhu is pursuing sensitivity analysis of grain

microstructures in terms of the stress-strain behavior of polycrystalline bcc Fe (e.g., uniform vs gradient grain sizes) by comparing molecular dynamics and crystal plasticity simulations.

As an example of sources of uncertainty sources in a sub-problem we outline below the sources of uncertainty for bottom-up and top-down pathways in uncertainty sub-problem 3 on BCC Fe crystal plasticity.

I. Bottom-up approach (Atomistics to Crystal Plasticity):

Approach 1: Vitek-Bassani-Groger [15-17]:

- Estimation of Peierls stress from 2D atomistic simulations and computing the effect of twinning-antitwinning asymmetry and non-glide stresses:
- Numerical algorithm used for energy minimization.
- Convergence criterion employed in incremental-loading, molecular-statics simulation
- Effect of boundary conditions employed.
- Inter-atomic potential: Single or double humped; degenerate or non-degenerate dislocation core.

Approach 2: Narayanan-McDowell-Zhu [18]:

- Estimation of kinkpair activation energy via 3D Nudged Elastic Band (NEB) calculations:
- Methodology for NEB implementation at finite stresses: Stress-controlled/Strain-controlled loading scheme.
- The effect of the atomistic simulation results rendering method, that brings in uncertainty into the estimation of the kink separation distance (a critical quantity that is used in the atomistic-continuum coupling).
- Accounting for dislocation density effect.
- Estimation of the numerical value of athermal resistance from atomistic computations.
- Inter-atomic potential: Accuracy of the EAM potential employed.
- Possible effects of twinning-antitwinning asymmetry and non-glide stresses, on kinkpair activation energy.
- Effect of zero-point crystalline vibrations (quantum effects) on kinkpair activation energy for low-temperatures.

II. Top-down approach (Experiments/Crystal Plasticity-to-Atomistics):

Approach 1: Patra-Zhu-McDowell [19-20]:

- Fitting of data points to exponential decay function for the temperature dependent non-Schmid coefficients
- Disagreement among experimental data sets
- Disagreement between experimental data and atomistic calculations regarding appropriate mechanisms and model forms

Comments on Likelihood Based UQ Method with Weighted Sampling

The likelihood based UQ method uses deterministic models in tandem with weighted sampling. The method can be characterized as a Structural Uncertainty Quantification technique. It is distinct in that it allows the model of interest to be informed by information in both a bottom-up and a top-down fashion.

The method can be used to evaluate the ability of a model to connect pieces of information. This is the simplest conceptualization of the method's purpose. By taking advantage of information at both the output level (top-down) and the input level (bottom-up), the method can test the degree to which these sources can be made to agree within the context of the model. The model serves in the role of a bridge between length scales.

Uncertain parameters and the assumed black box form of the model prevent a direct approach to the structural uncertainty.

A sampling based method, which executes the model over a sampling of different parameter values gives a more complete picture of uncertainty versus a single run on optimized parameter values. The model, if deterministic, requires that a single value be used for each parameter. This requirement holds for any single iteration of the model or any single run of the model, but different applications of the same model may favor different parameter values. Within a certain range, the parameters of the model can be varied without altering or violating the structural assumptions of the model. However, the output of the model is altered by these variations. Information that is not inherently captured by the model structure can be reflected within the model through the use of parameter values that maximize the agreement of the model and the additional information. The assumptions contained in the model form support the complete set of permutations of parameters, so to evaluate those assumptions the entire set of permutations must be included. In order to establish a connection between the structure of the model and validating or training data, the support from training data across parameter space must be evaluated. Therefore, the range of the uncertain parameters is included, and then weighted in a way that reflects a connection to a specific set of training data. It is also necessary to include the uncertainty of the training data as a consideration in this method in order to draw conclusions about the structural uncertainty.

The weighting referred to previously is better described as a likelihood based density estimate. A likelihood in a statistical model is tied to a parameter of the model. It denotes the degree to which the observed data supports the inference of a given value for that parameter. The weighting is indeed an estimate, because unlike a simple statistical model, the material models used here are separated from the validation data by a degree of inadequacy (which must be estimated).

Specific rudimentary numerical techniques are used here [least-squares linear regression modeling, polynomial interpolation in the surrogate model, orthogonal sampling methods], despite the presence of widely used methods of more sophistication [kriging, non-sampling methods such as orthogonal polynomial expansions, etc.]. This work uses the simplest workable techniques that are available as a matter of expediency. Future work, should this method prove viable, will have many avenues to explore for improving the choice of techniques made use of by this process.

Structure of the modeling effort and stepwise UQ procedure:

In mapping this method to a problem, it is helpful to hold the modeling effort of interest against the framework of this method. In doing so, the following key ingredients must be identified.

- a) Black box model

- b) Bottom-up information (parameter scale data)
- c) Top-down information (output scale data)
- d) Key calibration parameters of the model (with potential physical reinterpretations)

The absence of any of these four items would prevent the application of this technique. Additionally, the results of this technique will be specific to each combination of these four ingredients.

The individual steps of the procedure are as follows.

- 1) Identification of a Candidate model
- 2) Construction of the Black Box with theoretical boundaries for calibration parameters
- 3) Initial Sampling of Calibration Space
- 4) Per Datum Loss Functions from Likelihood
- 5) Mismatch of model structure from data as yardstick for level of discrimination in calibration space
- 6) Likelihood estimate across theoretically bounded calibration parameter space as a top-down structural uncertainty measurement
- 7) Loss function in calibration space
- 8) Single Bottom-up model (without BU calibration) case, $\theta \rightarrow x$ discrepancy
- 9) Multi (or with calibration) Bottom-up case, TDBU structural uncertainty

Task 2 Sources of uncertainty in model chains/linkages: Uncertainty Sub-Problems

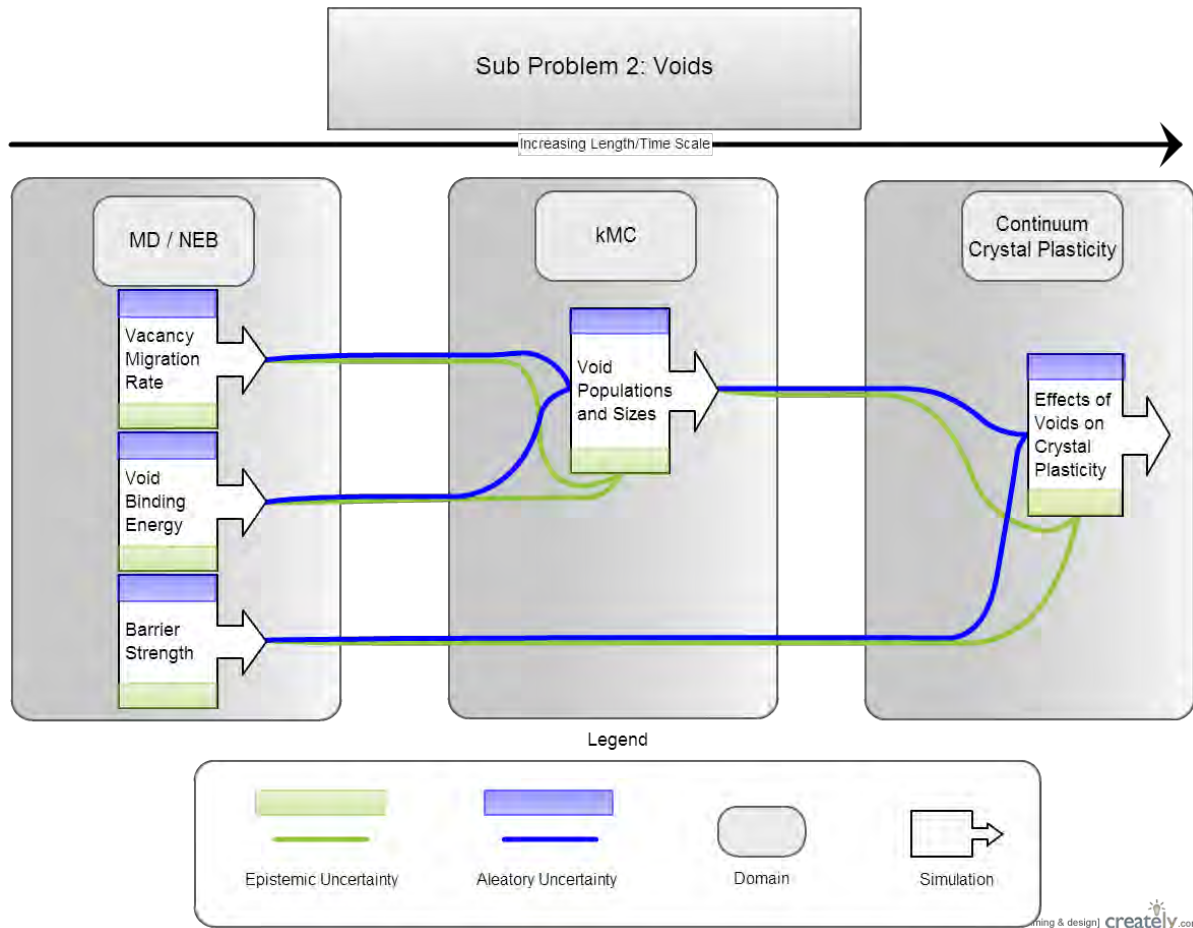
Dave McDowell and Yan Wang

Students: Aaron Tallman and Joel Blumer

Efforts focused on both further constitutive model development and framing of uncertainty sub-problems. The layout of uncertainty problems in terms of sources of uncertainty in model chains/linkages was completed in Q8.

Uncertainty Sub-Problems

The focus on uncertainty sub-problems shifted in the second year from one on sources of uncertainty (Task 1, described earlier) to configuration of the multiscale modeling chains (Task 2). Much progress was made in Q6-Q8 on assembling uncertainty sub-problems. The third year will focus on configuration of the uncertainty sub-problems to support pursuit of sensitivity studies and uncertainty quantification and propagation (Task 3).



Subproblem 3: Bottom-Up and Top-Down Uncertainty in Informing Crystal Plasticity for BCC Systems

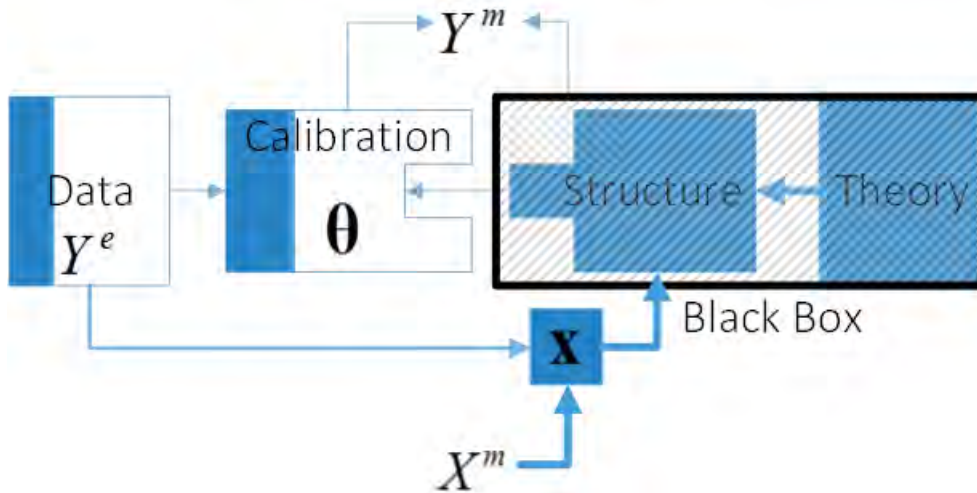
Calibration Based Structural Uncertainty Approach

This single Bottom-up model (without BU calibration) case, $\theta \rightarrow x$ discrepancy is the characterization of the top-down and bottom-up uncertainty. In the case where a single bottom-up model seeks to inform the calibration parameter values for the model in the black box, the bottom-up model is first assumed to be inflexible. This situation can arise if the bottom-up model cannot be calibrated or if the model results are the only information available. In this situation, a top-down and bottom-up uncertainty measure cannot be made. Instead, a linkage can be analyzed in terms of the amount of discrepancy that accompanies reinterpreting calibration parameters in the mesoscale model as physical parameters determined by a bottom scale model. This discrepancy can be found using the loss function described in 7). The discrepancy measure can be compared to the value of the loss function for other model cases, such as the self-discrepancy (for $\theta \rightarrow \hat{\theta}$ or MLE as connecting data), and the prior discrepancy, measured by replacing the objective function to a constant value (reflecting a uniform density in calibration parameter space). The prior self-discrepancy may be useful for identifying the effects of the calibration boundaries on the loss function.

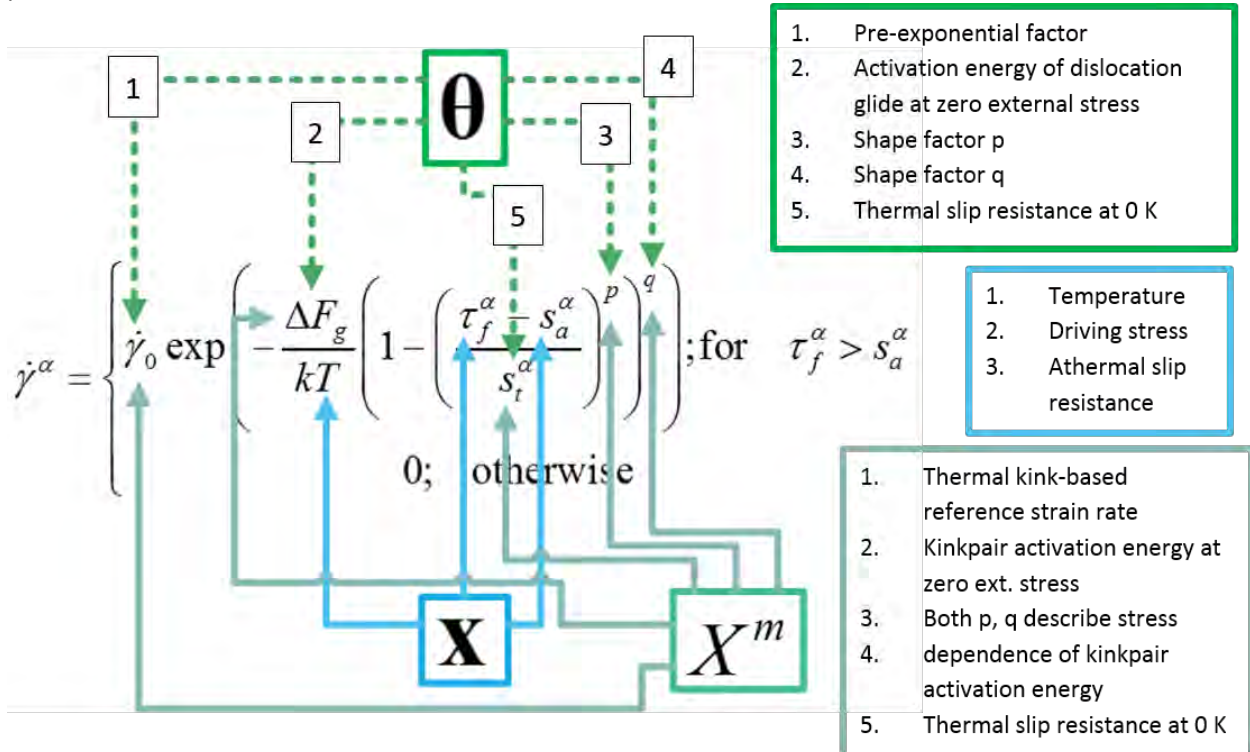
The following diagram is a conceptual picture of the modeling scenario. The model inside the black box is host to this reinterpretation of parameters.

Structural Bridge

$$\theta_i \xrightarrow{\text{becomes}} x_{n+1} = X^m$$



Here, the flow rule is shown with the specific parametric reinterpretations made in the scale bridging process.



Generalized Interval Probability Theory (GIPT) Based Approach

Validation of Crystal Plasticity models can be performed using experimental measurements conducted at higher length and time scales or from lower length and time scales, such as atomistic simulations of unit process mechanisms. Each of these methods has uncertainties involved that can limit the precision and certitude of the predictions made by the models once all of the uncertainty inherent in the model and the model validation process have been accounted for. In order to make use of all the information available, results will be coordinated from two crystal plasticity models that each use one of the validation schemes mentioned previously.

Each individual model needs to be calibrated with data that are imprecise, and for the Top-Down model, data on the deformation behavior of Fe from the literature will be analyzed in order to make confidence bands, and then the model will be calibrated to both of these idealized curves (top and bottom limits of the confidence interval). The Bottom-Up model will be calibrated to the nucleation energy of a kinkpair as measured by in-house atomistic modeling. This atomistic modeling has many internal sources of uncertainty, and the bottom-up model will be able to run using a confidence interval of values given by the model.

The scheme used for coordinating the predictions of these two models is being explored. Sensor Fusion, among other statistical modeling methods will be investigated. An ideal solution is to find a method that would have the capacity for manual belief to be applied to the weighting of the results of the different models. Eventually Generalized Intervals will be incorporated in order to separately treat aleatory and epistemic uncertainties between models where possible.

This subproblem will focus on using tested, familiar scientific modeling techniques in tandem with more sophisticated statistical and probabilistic modeling methods that may not be commonly associated with these fields of study in order to add additional depth to the simulations run in the future. The powerful data analysis techniques used in other data intensive fields can be a useful addition to the data heavy work of Uncertainty Quantification.

With regard to sub-problem 3, top-down and bottom-up validation methods are used in tandem to gain improved robustness in uncertainty measurements. In the case of study, two crystal plasticity models were taken and identified. One model had parameter estimates and validation via comparison with different sets of experimental data. The other model employed atomistic simulations to estimate parameters. The predictions of these models in previous work did not account for uncertainty. In the work of this past quarter, the uncertainty sources of the two models were measured and a methodology was planned for the fusion of these two models that accounts for uncertainty.

Model A: Top-down approach

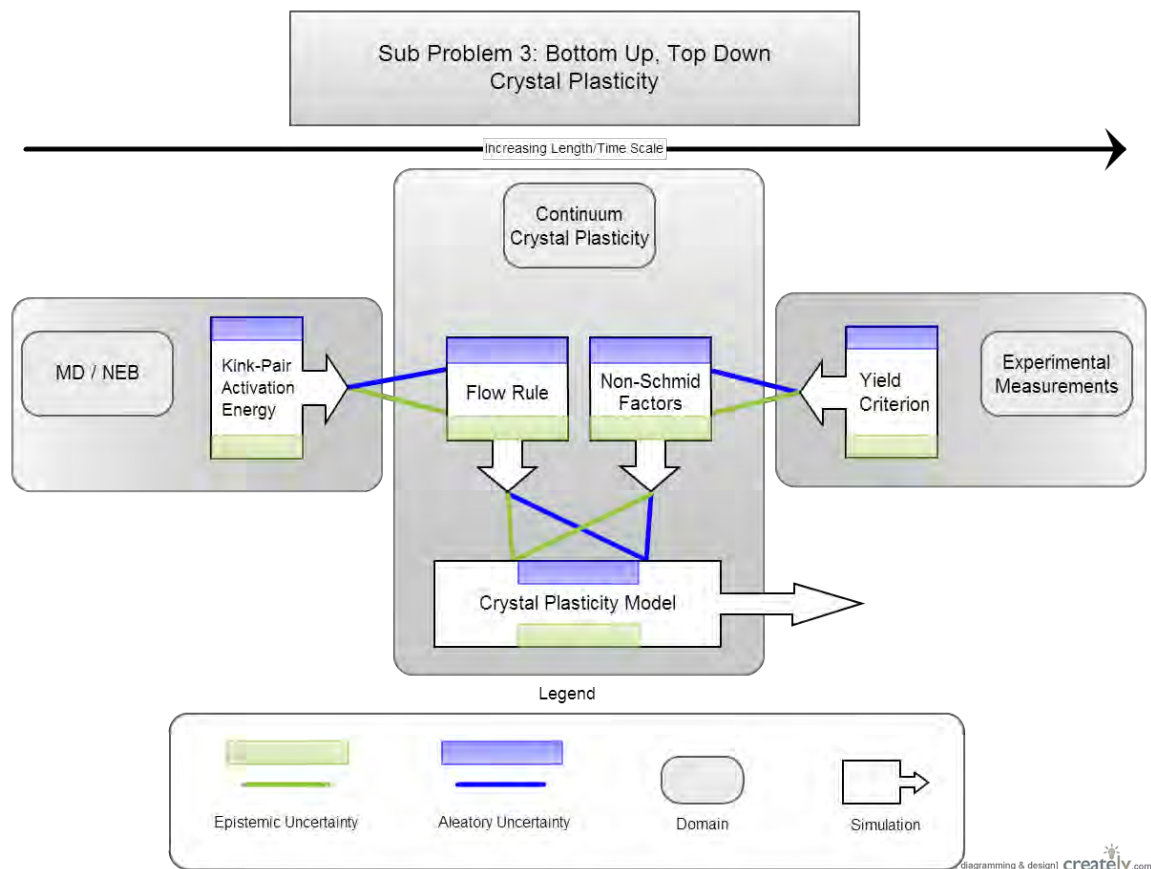
Uncertainty at the primary level originates in the measurements used for calibration and validation of the model. By using an interval treatment of uncertainty, two models can be constructed, one fit to the minimum values and one fit to the maximum values for the error bars or variability in measurements. In this way, the fitting parameters may also convey information related to the uncertainty in the data.

- Patra, A., Zhu, T. and McDowell, D.L., "Constitutive equations for modeling non-Schmid effects in single crystal bcc-Fe at low and ambient temperatures," *Int. J. Plasticity*, Vol. 59, 2014, pp. 1-14.

Model B: Bottom-up approach

Many parameters in the bottom-up model are based on values either found in literature, or those associated with atomistic modeling. The atomistic simulations contain uncertainty of their own, such as the choice and parameters of the EAM interatomic potential. The model must exercise a design of experiments compatible set of simulations in order to establish a rigorous interval for the uncertainty of the data.

- Narayanan, S., McDowell, D.L., and Zhu, T., "Crystal Plasticity Model for BCC Iron Atomistically Informed by Kinetics of Correlated Kinkpair Nucleation on Screw Dislocations," Journal of the Mechanics and Physics of Solids, Vol. 65, 2014, pp. 54-68.



Concerning Model Form Uncertainty

There is additionally the consideration of model form in the uncertainty quantification process. In the case here, this is not the most efficient or "strongest indicator" of actual uncertainty in the model chain. With the limitations imposed by finite processing power, prioritizing certain uncertainty sources for analysis may offer better results than an "all or nothing" approach. The reasons model form uncertainty will not be considered at the present stage for this model are as follows: Bayesian Model Averaging is an established method for calculating model form uncertainty, even removing it. This technique is very useful for simplistic statistical models. For the present case, the model is not a suitable candidate for this method, due to its processing expense and overall complexity. Additionally, the inclusion of scientifically

accepted knowledge built into the model might be compromised by BMA. Therefore, although it would be possible to address the uncertainty posed by questions such as the specific form to choose for the flow rule of model A are not directly addressed. Indeed, these questions may not be necessary if enough models are combined into the UQ regime in development. If Model form uncertainty is suspected as a large concern, the regime may be used to address this as well. By simply including the results of different forms of the same model (each form as a UQ pair of calibrations) in the final group of candidates. Moreover, the premise of our work is to focus on physically based models to the greatest extent possible, so the model forms selected embed expert knowledge at the outset. We view uncertainty of parameter estimation and fusion of information from bottom-up and top-down as the most pressing practical aspects of the present uncertainty analysis.

Models as Interpreters

Models interpret different sources of information, whether that information is in the form of experimental data, simulations on a different length and time scales, or even physical knowledge from scientific consensus. These interpreters each introduce different levels of uncertainty. Even the best model, however, cannot be more accurate or precise than the information that it is being used to interpret. Hence, the notion of a perfect model is elusive. In order to address this limitation, the proposition of using multiple models, multiple validation schemes, is essentially the attempt to coordinate a larger amount of information to address the quantity of interest.

Pertinence of Information

The pertinence of different information is a question of interest. Different models may give assenting or dissenting predictions. When they dissent, which model is correct? In order to maximize the pertinence of the output of the regime as a model system, confidence can be placed on models individually. This can also incorporate expert opinion, by means of attenuating the importance of models with predictions that seem less correct.

Method of Fusion

The method for fusing the output of these various models and experiments may depend on the values being addressed. For the case of these CCP simulations, the stress-strain relationship calculations may be combined in a number of ways. The simplest way would be to use the central limit theorem to synthesize the predictions to find a maximum likelihood estimate. This method could also be used to find a representative interval as well. Markov Chain Modeling could be used, if appropriate; however, the benefit of the simplest approach is that the predictions of the individual models are intact when incorporated into the final result. This makes the diagnosis (and repair) of poorly behaving individual models a much easier process. Additionally, as long as the uncertainty methods are performed and the Quantity of Interest remains unchanged, new models and therefore new information can be incorporated at minimal additional computational cost. Models are run independently; hence, even a network of models which each take days to run can be constructed.

Independence of Assumptions

An added benefit of an algebraic post-processing approach is that it allows models for a given process at selected length and time scales to remain independent of each other. This is critical if models with conflicting assumptions are used in tandem. Their results may be based on conflicting reasoning, but the

soundness of the separate models is not compromised by the combination of their results. This is in addition to the ease of use of this type of approach.

Summary

An approach to fuse different sources of information is established. The uncertainty of data is quantified and passed on through a pair of calibrations of each model. Each model communicates the predicted value and approximate uncertainty of its information. The contributors can be weighted according to confidence in the model, and the perceived pertinence of the information. If post processing of models executed in parallel is employed, contributing models maintain independence, can be included and excluded freely at minimal computational cost, and can be minimally invasive to the de facto modeling strategy.

Task 2. Uncertainty quantification based on Generalized Interval Probability

Quantifying Aleatory and Epistemic Uncertainties with Generalized Interval Probability Theory (GIPT)

Student: J. Blumer

Faculty: Y. Wang and D. McDowell

To be submitted to

ASME Journal of Verification, Validation & Uncertainty Quantification

A Bayesian Approach for Multiscale Model Validation with Imprecise Probability

Joel D. Blumer, David L. McDowell, Yan Wang

Georgia Institute of Technology, Atlanta, GA 30332

Abstract

To validate multiscale simulation models, it is necessary to consider evidence collected at a length scale that is different from the one at which a model predicts. In addition, epistemic and aleatory uncertainties need to be distinguished for more robust decision making. In this study, a Bayesian approach with generalized interval probability is taken for model parameter validation. A generalized interval Bayes' rule (GIBR) is used to combine the evidence and update belief in the validity of parameters. The sensitivity of completeness and soundness for interval range estimation in GIBR is investigated in comparison with Monte Carlo sampling. The method is first applied to validate the parameter set for a molecular dynamics simulation of defect formation due to radiation. It is then applied to combining the evidence from two models of crystal plasticity at different length scales.

Summary of the Study

Traditionally, sensitivity analysis is performed to assess the impact of epistemic uncertainty for modeling. Various methods such as variance-based global sensitivity analysis, local sensitivity analysis, Monte Carlo sampling, etc. have been developed. However, extensive computations are typically required in these methods to obtain the extent of variation. This prohibits their wide applications in large-scale simulations where each run of simulation is already costly. Alternatives such as Dempster-Shafer evidence theory, imprecise probability, random set, etc. have been developed to explicitly differentiate aleatory and epistemic uncertainty. As an extension of traditional probability theory, these approaches quantify uncertainty as a set of probability values. However, estimating the lower and upper bounds of

probabilities for probabilistic reasoning requires linear and nonlinear programming and is also computationally expensive.

In order to find efficient alternatives to sensitivity analysis to quantify epistemic uncertainty, in this study, generalized interval probability is used to represent the two components of uncertainty. A classical interval represents a set of real numbers with a pair of lower and upper bounds such as $[0.1,0.2]$. It can be used to quantify uncertainty when an exact value is unknown, but bounding values can be determined, for example, truncation errors in modeling and systemic errors in experimental measurement. Generalized intervals differ from traditional intervals primarily in that they allow the upper bound to precede the lower bound within the interval. In other words, both $[0.1,0.2]$ and $[0.2,0.1]$ are valid intervals. Combining generalized interval with probability, generalized interval probability provides simplified probabilistic calculus so that calculation and reasoning are much simpler than classical interval probability.

The aggregation of uncertain information can be done using Bayes' rule, where the belief obtained from one source (model prediction or experimental observation) is updated with the new evidence from another one. A similar Bayesian update approach based on generalized interval Bayes' rule (GIBR) was also proposed for interval-valued probabilities. In this study, the completeness and soundness of GIBR is investigated by comparing it with Monte Carlo simulations. A variation range estimation is called complete if it includes all possible scenarios and does not underestimate the range. In contrast, the estimation is called sound if all included scenarios are possible and the range is not overestimated. In other words, soundness denotes that a solution does not include any impossible values, whereas completeness means a solution does not exclude any possible values. The GIBR is defined as

$$\mathbf{P}(\gamma|\alpha) = \frac{\mathbf{P}(\alpha|\gamma) \cdot \mathbf{P}(\gamma)}{\mathit{dual} \int \mathbf{P}(\alpha|\gamma) d\gamma} \quad (1)$$

where $\mathbf{P}()$ is a generalized interval probability, and *dual* is an operator to switch interval bounds. For example, $\mathit{dual}[0.1,0.2] = [0.2,0.1]$ and $\mathit{dual}[0.2,0.1] = [0.1,0.2]$. Notice that the algebraic form of GIBR is very similar to classical Bayes' rule, except for the application of *dual* operator on the interval probabilities. It is important to notice that when intervals degenerate to precise real values, GIBR converges to classical Bayes' rule. An application of GIBR is

$$\mathbf{P}(\gamma|\alpha) = \frac{\int \mathbf{P}(\alpha|\beta) \cdot \mathbf{P}(\beta|\gamma) d\beta \cdot \mathbf{P}(\gamma)}{\mathit{dual} \int \int \mathbf{P}(\alpha|\beta) \cdot \mathbf{P}(\beta|\gamma) \cdot \mathbf{P}(\gamma) d\beta d\gamma} \quad (2)$$

where causal relationships among variables are captured. The major advantages of GIBR over other definitions of Bayes' rule for interval probability are the simplicity of calculation without the need of using optimization to estimate interval bounds for posteriors as in other approaches and its resemblance to the classical Bayes' rule for ease of use. A logic coherence constraint is typically required when assigning interval values to probability, which states that the sum of all interval probabilities within the sample space is one (i.e., $[1,1]$). This constraint is more restrictive than the coherence constraints proposed in other forms of imprecise probability. This constraints takes advantage of the algebraic convenience in a generalized interval, where proper and improper intervals co-exist. For instance, $[0.1,0.2]$ is proper, whereas $[0.2,0.1]$ is improper. The existence of improper intervals allows for reduction of interval range, according to Kaucher interval arithmetic. Therefore, it is possible that the sum of proper and improper interval probabilities is one.

To verify the completeness and soundness of GIBR, Monte Carlo sampling is applied. Figure 6 shows an example when numerical values are randomly assigned to Eq. (2). The two solid straight lines indicate the bounds of the posterior interval probability estimated by GIBR, in comparison with the histogram of posteriors from 1 million Monte Carlo simulation runs of classical Bayes' rule with priors and likelihoods uniformly sampled from the given intervals. The interval estimation from GIBR is sound but not complete. As interval priors and likelihoods reduce the interval widths from the original ones (Fig. 6-a) to halves (Fig. 6-b) and quarters (Fig. 6-c), the completeness improves. The interval widths are 57.19%, 58.72%, and 59.06% respectively of the widths from Monte Carlo sampling. The majority of Monte Carlo samples (more than 90%) are included by the GIBR interval estimates. Normal distributions are also applied in the sampling (Fig. 6-d), where 99.45% of samples are included in the interval estimate.

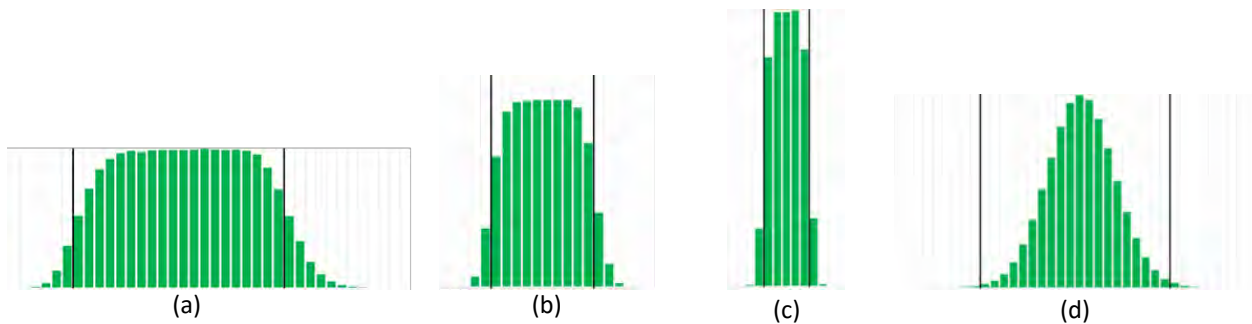


Fig. 6: Comparison between interval posterior estimates from GIBR and the ones from Monte Carlo (M.C.) simulation where samples are drawn from interval priors and likelihoods. (a) Original prior and likelihood widths with samples drawn from uniform distributions (91.73% of M.C. samples are included in GIBR interval. GIBR interval width is 57.19% of M.C. width). (b) Halves of original prior and likelihood widths with samples drawn from uniform distributions (91.24% of M.C. samples are included in GIBR interval. GIBR interval width is 58.72% of M.C. width). (c) Quarters of original prior and likelihood widths with samples drawn from uniform distributions (91.05% of M.C. samples are included in GIBR interval. GIBR interval width is 59.06% of M.C. width). (d) Original prior and likelihood widths with samples drawn from normal distributions (99.45% of M.C. samples are included in GIBR interval. GIBR interval width is 58.23% of M.C. width).

Similar to classical Bayes' rule, the challenge of applying GIBR in information aggregation is when there is a lack of information. In the case that no information is available and total ignorance is present, interval probability takes an interval value of $[0,1]$. When a causal relationship is imprecise, interval likelihoods are taken. When there is absolutely no information about the causal relationship, $[0,1]$ is assigned. When total ignorance is considered in GIBR with $[0,1]$ assignments to likelihoods, it is intuitive that no update is obtained without any new information.

To illustrate with a numerical example of multiscale model validation, where molecular dynamics simulation models of point defect because of irradiation are validated. Radiation induced swelling $(\Delta l/l)/n$ and resistivity change $\Delta\rho/n$ are measured at macroscale to compare with the simulation predictions at atomistic scale. The posterior of model parameters θ after experimental observations are obtained based on GIBR as in

$$\mathbf{P}\left(\theta \mid \frac{\Delta\rho}{n} \cap \frac{\Delta\ell/\ell}{n}\right) = \frac{\int \int \left[\mathbf{P}\left(\frac{\Delta\rho}{n} \mid T_m\right) \cdot \mathbf{P}\left(\frac{\Delta\ell/\ell}{n} \mid T_m\right) \cdot \mathbf{P}(T_m | T_d) \cdot \mathbf{P}(T_d | \theta) \right] dT_d dT_m \cdot \mathbf{P}(\theta)}{\text{dual} \int \int \int \left[\mathbf{P}\left(\frac{\Delta\rho}{n} \mid T_m\right) \cdot \mathbf{P}\left(\frac{\Delta\ell/\ell}{n} \mid T_m\right) \cdot \mathbf{P}(T_m | T_d) \cdot \mathbf{P}(T_d | \theta) \cdot \mathbf{P}(\theta) \right] dT_d dT_m d\theta} \quad (3)$$

where transferred energy T_m and damage threshold T_d are used to build causal relationships. Suppose that

$$\begin{aligned} \mathbf{P}(T_m = 70eV | T_d > 70eV) &= [0,0], \\ \mathbf{P}(T_m = 100eV | T_d > 70eV) &= [0,1], \\ \mathbf{P}(T_m = 70eV | T_d > 70eV) &= [1,0], \\ \mathbf{P}(T_d \leq 70eV | \theta^C) &= [0,1], \text{ and} \\ \mathbf{P}(T_d > 70eV | \theta^C) &= [1,0]. \end{aligned}$$

The posterior probability is the same as the prior. Total ignorance indicates that causal relationship is unknown in the chain of reasoning. No belief update is expected. Monte Carlo sampling however indicates the underestimation of the range for posterior in the case of total ignorance. The logic coherence constraint is applied in the above example. Arguably the constraint imposed for total ignorance is overly restrictive. For three or more possible outcomes from one action, it is difficult to justify that zero knowledge about the probability for one outcome would lead to the probability of zero on another. In addition, different assignments of [0,0], [0,1], and [1,0] to $\mathbf{P}(T_m | T_d)$ lead to different results. Therefore a more reasonable assignment is to have all probabilities be [0,1], and the logic coherence constraint should not be applied to the case of total ignorance. Experiments showed some improvement of completeness when all probabilities are assigned to be [0,1].

Two models that predict the yield strength of bcc iron are used in a case study for model information aggregation. The first one is a finite element model for dislocation density crystal plasticity that considers non-Schmid effects in both crystal orientation and in the tension-compression asymmetry at initial yield, whereas the second one is a crystal viscoplasticity model that accounts for temperature-dependence in the non-Schmid parameters. The lack of prior knowledge about orientation of the studied system is considered as epistemic uncertainty. Therefore interval probabilities are assigned. The aggregation can be done via either

$$\mathbf{P}(y_{m1} | y_{m2}) = \frac{\int \mathbf{P}(y_{m1} | t) \cdot \mathbf{P}(t | y_{m2}) dt \cdot \mathbf{P}(y_{m1})}{\text{dual} \int \int \mathbf{P}(y_{m1} | t) \cdot \mathbf{P}(t | y_{m2}) \cdot \mathbf{P}(y_{m1}) dt dy_{m1}} \quad (4)$$

or

$$\mathbf{P}(y_{m2} | y_{m1}) = \frac{\int \mathbf{P}(y_{m2} | t) \cdot \mathbf{P}(t | y_{m1}) dt \cdot \mathbf{P}(y_{m2})}{\text{dual} \int \int \mathbf{P}(y_{m2} | t) \cdot \mathbf{P}(t | y_{m1}) \cdot \mathbf{P}(y_{m2}) dt dy_{m2}} \quad (5)$$

with y_{m1} and y_{m2} as predictions of yield from model 1 and model 2 respectively at temperature t . The results are also sensitively dependent upon the choices of proper and improper intervals during the assignments.

Interval-valued Kullback-Leibler (KL) divergence is also proposed to validate model with imprecise probability. With interval probabilities \mathbf{p}_i 's and \mathbf{q}_i 's, interval-valued KL divergence between the two is defined as

$$\mathbf{D}_{KL}(\mathbf{p} | \mathbf{q}) = \sum_i \mathbf{p}_i \ln \frac{\mathbf{p}_i}{\mathbf{q}_i} \quad \text{and} \quad \mathbf{D}_{KL}(\mathbf{q} | \mathbf{p}) = \sum_i \mathbf{q}_i \ln \frac{\mathbf{q}_i}{\mathbf{p}_i}$$

The symmetric one is

$$D_{KLS}(\mathbf{p}, \mathbf{q}) = \text{pro}(D_{KL}(\mathbf{p}|\mathbf{q})) + \text{pro}(D_{KL}(\mathbf{q}|\mathbf{p}))$$

where $\text{pro}(\mathbf{p})$ returns a proper version of interval \mathbf{p} . A smaller value of KL divergence indicates that model can be validated by experiment with a higher level of consistency. With interval-valued KL divergence, the imprecision is quantified by intervals. The cases of overlap or inclusion between two interval-valued KL divergences from two models imply the lack of confidence about the assertion about which model is more valid.

In summary, generalized interval probability provides a computationally efficient alternative to traditional sensitivity analysis for epistemic uncertainty. The unique algebraic property of generalized interval allows for simple calculation such as Bayes' rule that is similar to the one in classical probability. Generalized interval Bayes' rule ensures soundness of interval range estimation of posterior probability under epistemic uncertainty at the expense of completeness. Wide interval probabilities with large epistemic uncertainty lead to underestimation of interval ranges during calculation. Additional sensitivity analysis for assigning proper and improper interval probabilities is thus recommended to improve completeness. As the widths of input intervals reduce, the extent of underestimation also reduces with more complete estimation. When the widths reduce to zero, it converges to classical Bayes' rule. The total ignorance representation [0,1] in likelihoods does not provide more advantage over the equal-probability approach used in classical probability. In addition, the developed Bayesian approach for cross-scale information aggregation and model validation is generally applicable for both imprecise probability and classical probability. The Bayesian aggregation approach for multiscale uncertainty quantification with the presence of both aleatory and epistemic uncertainty needs further investigation.

Task 3 Sensitivity studies

Sensitivity studies comprises the bulk of the third year effort, along with configuration of the model chains for the three uncertainty sub-problems.

Summary of Accomplishments, September 1, 2012 – August 31, 2015

Primary advisors and students supported are as follows:

Professor: T. Zhu

Atomistics and unit processes

Informing crystal plasticity

Informing KMC

Uncertainty of interatomic potentials, boundary conditions, schemes, etc.

Student: Zhi Zeng

Professor: C. Deo

KMC and event frequencies for mechanisms

Uncertainty of events, frequencies, unit processes, interactions, etc.

Informing crystal plasticity

Students: Each supported ½ time on this project

Richard (Trey) Hoffman

Alex Moore, Completed MS Degree, now PhD student

Professors: D.L. McDowell and Y. Wang

Crystal plasticity

Hierarchical multiscale modeling chains

Interval probability estimates and schemes

Oversight and collaborative execution (with students 1 and 2) of uncertainty propagation and mitigation

Students: Aaron Tallman (fall 2012-present) and Joel Blumer (graduated with MS degree in 2014).

Some of the multiscale models in uncertainty sub-problem 3 are built upon foundations of models built with support of the prior NEUP award DE-AC07-05ID14517 09-269, supporting the PhD theses of Sankar Narayanan (graduated in May 2014) and Anirban Patra (graduated in December 2013).

It is expected that building on the foundations of this NEAMS funding, all three uncertainty sub-problems will be fleshed out fully in the collaborative continued doctoral theses and joint papers by the students and faculty supported by this program, as outlined in Section ?. Moreover, an internship is being pursued at Sandia National Laboratories for Aaron Tallman, who is a key collaborating PhD student in pursuing collaborative execution of the following three multiscale uncertainty sub-problems:

- 1. Interstitial Loop/Dislocation Interactions in Irradiated Fe Alloys**
- 2. Void Nucleation, Growth and Interactions with Dislocations in Irradiated Fe Alloys**
- 3. Bottom-Up and Top-Down Uncertainty in Informing Crystal Plasticity for BCC Systems**

Conferences Attended

- Various team members (D.L. McDowell served as General Chair), Society of Engineering Science 49th Annual Technical Meeting, Atlanta, GA, Oct. 10-12, 2012
- Yan Wang, The 2nd World Congress on Integrated Computational Materials Engineering (ICME'13), July 7-11, 2013, Salt Lake City, Utah
- David McDowell, MRS Fall Meeting, Boston, MA, Nov. 25-30, 2012

- David McDowell and Ting Zhu, TMS annual meeting, San Antonio, TX, March 3-7, 2013
- Chaitanya Deo and David McDowell, ANS Annual Meeting, Atlanta, GA, June 16-20, 2013
- R. Hoffman and C. Deo, Nuclear Fuels (MMSNF) 2013 Workshop, October 14-16 2013, Chicago, IL.
- David McDowell and Ting Zhu, MS&T annual meeting, Montreal, Canada, Oct. 27-31, 2013
- Chaitanya Deo and David McDowell, MRS Fall Meeting, Boston, MA, Dec. 1-6, 2013
- David McDowell and Ting Zhu, 7th International conference on Multiscale Materials Modeling, Berkeley, CA, Oct. 6-10, 2014.
- Chaitanya Deo, David McDowell, Zhi Zeng, and Ting Zhu, TMS annual meeting, San Diego, CA, Feb. 16-20, 2014.
- Chaitanya Deo, Trey Hoffman, and David McDowell, 17th U. S. National Congress on Theoretical and Applied Mechanics, Lansing, MI, June 15-20, 2014.
- Chaitanya Deo and Trey Hoffman, American Nuclear Society (ANS), Reno, NV, June 15-19, 2014.
- Yan Wang, The 2nd International Conference on Vulnerability and Risk Analysis and Management (ICVRAM2014) & 6th International Symposium on Uncertainty Modeling and Analysis (ISUMA2014), July 13-16, 2014, Liverpool, UK
- Chaitanya Deo and David McDowell, MRS Fall Meeting, Boston, MA, Nov. 30-Dec. 5, 2014.
- Chaitanya Deo and Alex Moore, MRS Spring Meeting, San Francisco, CA, April 6-10, 2015.
- David McDowell, 4th International Conference on Material Modeling, Berkeley, CA, May 27-29, 2015.
- David McDowell, ICME 3rd World Congress, Colorado Springs, CO, May 31-June 4, 2015.
- Zhi Zeng and Ting Zhu, ASME Materials and Applied Mechanics conference, Seattle, WA June 29-July 1, 2015

Conference Presentations

T. Zhu, "Deformation and Fracture Mechanisms in Gradient Nano-Grained Metals" TMS annual conference in San Antonio, TX, March 2013.

Wang Y., McDowell D.L., Tallman A.E. "Cross-scale, cross-domain model validation based on generalized hidden Markov model and generalized interval Bayes' rule" 2nd World Congress on Integrated Computational Materials Engineering (ICME 13), July 7-11, 2013, Salt Lake City, Utah.

Wang Y. (August 2013) "Validation of Atomistic Simulation under Aleatory and Epistemic Uncertainties", National Institute of Standards & Technology, Gaithersburg, Maryland, August 2013.

R. Hoffman, R. Behera, and C. Deo, "Kinetic Monte Carlo Study of Oxygen Defect Migration in Urania Fuel." Materials Modeling and Simulation for Nuclear Fuels (MMSNF) 2013 Workshop, October 14-16 2013, Chicago, Illinois (poster).

Hoffman, R.T., Bahera, R., Deo, C.S., "Kinetic Monte Carlo study of oxygen defect migration in urania fuel," Materials Modeling and Simulation for Nuclear Fuels, Chicago, IL, October 14-16, 2013.

Narayanan, S., Zhu, T. and McDowell, D.L., "Crystal Plasticity Model for BCC Iron Atomistically Informed by the Kinetics of Correlated Kinkpair Nucleation," MS&T '13, Montreal, Quebec, Canada, October 27-31, 2013.

Patra, A., Zhu, T., and McDowell, D.L., "Constitutive Equations for Dislocation Core Spreading in BCC-Fe Accounting for Dislocation-Dislocation Interactions and Finite Temperature Effects," MS&T '13, Montreal, Quebec, Canada, October 27-31, 2013.

T. Zhu, "Crystal Plasticity Model for BCC Iron Atomistically Informed by Kinetics of Correlated Kinkpair Nucleation on Screw Dislocations," TMS annual conference in San Diego, CA, February 2014.

Z. Zeng, T. Zhu, "Atomistic and electron tomography study of 3D dislocation-grain boundary interaction in BCC metals," TMS annual conference in San Diego, CA, February 2014.

R. Hoffman and C. Deo, "Kinetic Monte Carlo Study of Fission Gas and Grain Growth in Nuclear Materials." TMS Annual Meeting February, 2014 (poster).

R. Hoffman, R. Behera, and C. Deo, "Atomistic Investigation of Ionic Conductivity in Thorium-doped Urania Fuel", TMS Annual Meeting February 2014.

Deo, C., "Calculation of Threshold Energy", TMS annual conference in San Diego, CA, February 2014.

Narayanan, S., McDowell, D.L., and Zhu, T., "Crystal Plasticity Model for BCC Iron Atomistically Informed by Kinetics of Correlated Kinkpair Nucleation on Screw Dislocations," TMS 2014, San Diego, CA, Feb. 18, 2014.

Deo, C., Beeler, B., Okuniewski, M., Baskes, M., "Atomistic Modeling of Radiation Damage in bcc Uranium," 2014 TMS Annual Meeting & Exhibition, Progress Towards Rational Materials Design in the Three Decades Since the Invention of the Embedded Atom Method: An MPMD Symposium in Honor of Dr. Michael I Baskes, San Diego, CA February 2014.

Wang Y., McDowell D.L., Blumer J.D., Tallman A.E. "Quantification of model form uncertainty in molecule dynamics simulation." 2014 Society for Industrial & Applied Mathematics (SIAM) Conference on Uncertainty Quantification, Savannah, GA, March 30-April 3, 2014.

McDowell, D.L., "Bridging Mesoscale Gaps to Enable Design of Materials at Extremes," Opening Plenary Lecture, Mach Conference 2015, Annapolis, MD, April 9-11, 2014.

R. Hoffman and C. Deo, "Use of the Potts Model to Analyze Nuclear Materials" The 17th U. S. National Congress on Theoretical and Applied Mechanics, June 15-20 2014, Lansing, Michigan.

Moore A., Chen, E., Deo, C., "Atomistic Study and Characterization of Metallic Uranium Interphases and Grain Boundaries," Symposium on Multiscale Modeling and Experiments on Microstructural Evolution in Nuclear Materials, MRS Spring Meeting, San Francisco, CA, April 6-10, 2015.

Tallman, A., Blumer, J., Wang, Y., Narayanan, S., Zhu, T. and McDowell, D.L., "Bottom-up and Top-down Uncertainty Quantification of bcc Fe Single Crystal Plasticity," ICME 3rd World Congress, Colorado Springs, CO, June 3, 2015 (invited).

McDowell, D.L., "Rectifying Bottom-Up and Top-Down Uncertainties in Multiscale Modeling: Scientific and Engineering Aspects Relevant to ICME Multilevel Materials Design and Development," ICME 3rd World Congress, Colorado Springs, CO, June 4, 2015 (plenary).

Conference Papers

Wang Y., McDowell D.L., Tallman A.E. "Cross-scale, cross-domain model validation based on generalized hidden Markov model and generalized interval Bayes' rule." Proceedings of the 2nd World Congress on Integrated Computational Materials Engineering (ICME'13), July 7-11, 2013, Salt Lake City, Utah, pp.149-154.

Tallman A.E., Blumer J.D., Wang Y., and McDowell D.L. "Multiscale model validation based on generalized interval Bayes' rule and its application in molecular dynamics simulation." Proceedings of 2014 ASME International Design Engineering Technical Conferences & Computers and Information in Engineering Conference (IDETC/CIE2014), Aug. 17-20, 2014, Buffalo, New York, Paper No. DETC2014-35126.

Wang Y. "Training generalized hidden Markov model with interval probability parameters." Proceedings of 2nd International Conference on Vulnerability and Risk Analysis and Management (ICVRAM2014) & 6th International Symposium on Uncertainty Modeling and Analysis (ISUMA2014), July 13-16, 2014, Liverpool, UK.

Journal Articles

Submitted and Accepted During this Grant Period

Atomistic modeling of high temperature uranium-zirconium alloys structure and thermodynamics, A. Moore, B. Beeler, C. Deo, M. I. Baskes and M. A. Okuniewski, submitted to Journal of Nuclear Materials June 2015, Accepted for Publication September 2015.

Narayanan, S., McDowell, D.L., and Zhu, T., "Crystal Plasticity Model for BCC Iron Atomistically Informed by Kinetics of Correlated Kinkpair Nucleation on Screw Dislocations," Journal of the Mechanics and Physics of Solids, Vol. 65, 2014, pp. 54-68.

Patra, A., Zhu, T. and McDowell, D.L., "Constitutive equations for modeling non-Schmid effects in single crystal bcc-Fe at low and ambient temperatures," Int. J. Plasticity, Vol. 59, 2014, pp. 1-14.

J. W. Wang, S. Narayanan, J. Y. Huang, Z. Zhang, T. Zhu and S. X. Mao. Atomic-scale dynamic process of deformation-induced stacking fault tetrahedra in gold nanocrystals. Nature Communications, 4, 2340 (2013)

Journal articles submitted

Bahera, R.K., Watanabe, T, Andersson, D.A., Uberuaga, B.P., and Deo, C.S., "Role of O/M ratio and O-O binding energy on the diffusion of oxygen interstitials in UO_{2+x} using kinetic Monte Carlo Simulations," submitted to Journal of Nuclear Materials, August 2015.

Journal articles in preparation

- A Bayesian approach for multiscale model validation with imprecise probability
Blumer, J.D., McDowell, D.L., and Wang, Y.
- Sensitivity analysis of Point Defect Balance Equations

- R. Hoffman, A. Tallman, C.S. Deo and D.L. McDowell
- Diffusion of oxygen vacancies in doped ceria and Urania - draft under preparation for submission to the Journal of Nuclear Materials
R. Hoffman and C.S. Deo
 - Structural Uncertainty Quantification in Rate Law simulation of bcc metal irradiation-void nucleation and growth
R. Hoffman, A. Tallman, A. Moore, C. Deo, D.L. McDowell
 - Rate Law simulation of bcc Fe irradiation-void nucleation and growth, with Uncertainty Propagation through Crystal Plasticity modeling of irradiated bcc Fe
A. Tallman, T. Hoffman, A. Moore, Y. Wang, C. Deo, D.L. McDowell
 - Uncertainty Propagation within MD-informed Crystal Plasticity Modeling of Mobile and Immobile Interstitial Loops in Irradiated bcc Fe
Z. Zeng, A. Tallman, T. Zhu, Y. Wang, D.L. McDowell
 - Top-Down and Bottom-Up Uncertainty Quantification of MD-informed Crystal Plasticity Modeling of Mobile and Immobile Interstitial Loops in Irradiated bcc Fe
A. Tallman, Z. Zeng, T. Zhu, Y. Wang, D. L. McDowell
 - Bottom-up and top-down uncertainty quantification of bcc Fe plasticity and dislocation-interstitial loop interactions
A.E. Tallman, Z. Zeng, C. Sobie, Y. Wang, L. Capolungo, T. Zhu, D.L. McDowell
 - Calibration Based Structural Uncertainty Quantification of a Top-Down and Bottom-Up Crystal Plasticity Model of bcc Fe
Aaron Tallman, Yan Wang, David L. McDowell

Theses Awarded

Blumer, J. "Cross-Scale Model Validation with Aleatory and Epistemic Uncertainty," M.S. Thesis, Georgia Institute of Technology, May 2015

Invited Seminars

Wang Y. (August 2013) "Validation of Atomistic Simulation under Aleatory and Epistemic Uncertainties," National Institute of Standards & Technology Workshop on Atomistic Simulations for Industrial Needs, Gaithersburg, Maryland.

Wang Y., "Quantifying model form uncertainty in molecular dynamics simulation." December 16-17, 2013, invited presentation, University of Minnesota, Institute for Mathematics and its Applications, Minneapolis, Minnesota, Dec. 16-17, 2013.

McDowell, D.L., "Modeling Inelastic Behavior of Metals at Multiple Scales for Multiple Purposes," George Washington University, April 8, 2014.

McDowell, D.L., "Modeling Inelastic Behavior of Metals at Multiple Scales for Multiple Purposes," Arizona State University, October 3, 2014.

Wang Y., "Uncertainty Quantification for Reliable Atomistic Simulation," Colorado School of Mines. Dec. 2014.

Conference, Symposium and Workshop Organization

Wang, Y., Mini Symposium "Model Form Uncertainty in Modeling, Simulation and Analysis" at 2014 SIAM Conference on Uncertainty Quantification, Savannah, Georgia, with 12 presentations (co-organizers: Laura Swiler, Sankaran Mahadevan)

McDowell, D.L., Chair, 49th Annual Technical Meeting of the Society of Engineering Science (SES), Georgia Tech Hotel, Oct. 10-12, 2012 (420 participants).

McDowell, D.L., Member, Scientific Committee, 17th U.S. National Congress on Theoretical and Applied Mechanics, Michigan State University, East Lansing, MI, June 16-20, 2014 (along with T. Hughes and M. Sacks, Univ. Texas-Austin, M. Abeyaratne, MIT, F. Moon, Cornell, and A. Smits, Princeton).

McDowell, D.L., Co-organizer (with J. Neugebauer, D. Wu, P. Gumbsch, K. Rajan, and V. Bulatov), Symposium on Multiscale Simulations and Modeling Integrated Materials Engineering, with Bulatov et al., 7th Int. Conference on Multiscale Materials Modeling, 2014, Berkeley, CA, Oct. 6-10, 2014.

McDowell, D.L., Co-organizer (with K. Hackl), Symposium on Multiscale Modeling (multi-day), 4th Int. Conf. on Materials Modeling, Berkeley, CA, May 27-29, 2015.

May 8, 2014 Sandia Review of the Georgia Tech NEAMS Program

In the first year, the co-PIs attended several conferences and presented results. PI D.L. McDowell traveled to both PNNL and INL to discuss research within this program to both modeling and simulation and experimental groups with regard to collaboration. Laura Swiler from Sandia visited Georgia Tech on February 7, 2013 for a project review and summary of first year plans.

D.L. McDowell coordinated with L. Swiler at Sandia-Albuquerque to hold a ½ day telecom review of this NEAMS program with a Sandia team covering aspects of atomistic modeling, multiscale modeling, and uncertainty May 8, 2014.

Objectives:

- Mid-course project reporting and feedback from Sandia
- Integrate more closely with Sandia uncertainty modeling efforts
- Identify potential collaborations

Agenda

11:00 am Welcome and Introductions, Sandia Interests – Dave McDowell and Laura Swiler

11:15 am

Overview of Georgia Tech NEAMS program

- o Overall objectives and timeline – Dave McDowell (15 minutes)
- o Multiscale models
 - MD Knock on – CD and students (10 minutes)
 - NEB and unit processes; ab initio for core interactions – Ting Zhu and students (15 minutes)
 - KMC for cooperative processes – CD and students (15 minutes)
 - Mechanism-based crystal plasticity – Dave McDowell and Aaron Tallman (15 minutes)
- o Generalized Interval probability theory and Markov chains
 - General principles – Yan Wang (20 minutes)
 - MD knock-on simulations for Frenkel pair formation – Yan Wang and students (15 minutes)

1:10 pm - Outline and describe uncertainty subproblems – Aaron Tallman and Joel Blumer (20 minutes)
Summary of progress – Dave McDowell (5 minutes)

1:35 pm - General discussion, Sandia feedback and guidance

Adjourn 2:00 pm

Attendees: Entire GT team

Georgia Tech: Entire team of faculty and graduate students

Sandia: Laura Swiler and team of atomistics modelers and uncertainty experts



Uncertainty Quantification and Management for Multiscale Nuclear Materials Modeling

OVERVIEW

Purpose: The project incorporated uncertainty and error assessments within the length and time scales appropriate to each model to assess how this propagates through a chain of multiscale models for irradiated BCC Fe-Cr ferritic/martensitic steels. The goal was to establish a consistent methodology to quantify uncertainty in model parameters and related inputs and assumptions, as well as numerical implementation, and to develop a means to manage propagation of uncertainty in multiscale modeling.

Objectives:

- Uncertainty quantification for each model (atomistic, KMC, continuum crystal plasticity) comprising a multiscale modeling framework for mechanical behavior of irradiated Fe-Cr ferritic alloys.
- Methods to address propagation of uncertainty in multiscale model chains, with focus on three distinct sub-problems.
- Sensitivity studies and parametric evaluation of uncertainty on model problems concerning irradiation effects on mechanical behavior of Fe-Cr ferritic alloys.

IMPACT

Logical Path: Building on a prior NEUP multiscale modeling program for irradiated Fe-Cr ferritic alloys, this effort addressed uncertainty quantification (UQ) and propagation associated with model prediction of material behaviors at and across different scales to provide cross-domain and cross-scale information representation and inference.

Outcomes: Understanding and improving microstructural mechanical stability in metals and alloys is central to the development of high strength and high ductility materials for cladding and core structures in advanced fast reactors. Novel methods based on generalized interval probability and pseudolikelihood were developed and continue to be refined in several doctoral theses for three uncertainty sub-problems involving linkages between quantum mechanics, atomistics, kinetic Monte Carlo and finite element crystal plasticity models. The bulk of the UQ is built on conventional uncertainty representations pursued using Latin Hypercube Sampling methods with Gaussian Process modeling. These methods are applicable to broad ranges of applications involving chains of models for phenomena occurring at disparate length and time scales.

DETAILS

Principal Investigator: David L. McDowell
Institution: Georgia Institute of Technology

Collaborators: Co-Pis Chaitanya Deo, Ting Zhu, Yan Wang, Georgia Tech

Duration: 3 years, 9/1/12-8/31/15

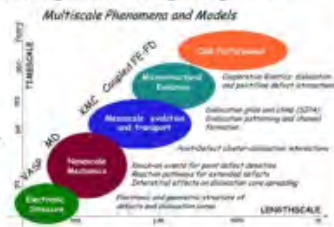
Total Funding Level: \$743,444

TPOC: Laura Swiler, Sandia

Federal Manager: Tansel Selekler

Workscope: NEAMS-3

PICSNE Workpackage #: NU-12-GA-GT-0401-03



RESULTS

Results: Multiscale uncertainty sub-problems pursued using pseudo-likelihood UQ: (i) Interstitial Loop/Dislocation Interactions in Irradiated Fe Alloys, (ii) Void Nucleation, Growth and Interactions with Dislocations in Irradiated Fe Alloys, and (iii) Bottom-Up and Top-Down Uncertainty in Informing Crystal Plasticity for BCC crystals/polycrystals.

Accomplishments: Completion of all tasks, with focus on uncertainty sub-problems superseding emphasis on year 3 sensitivity studies. Outcomes include 4 journal articles published, 1 submitted, 9 in preparation; 20 conference presentations; several PhD theses in progress.

Blumer, J. "Cross-Scale Model Validation with Aleatory and Epistemic Uncertainty," M.S. Thesis, Georgia Institute of Technology, May 2015

Presentations: Tallman, A., Blumer, J., Wang, Y., Narayanan, S., Zhu, T. and McDowell, D.L., "Bottom-up and Top-down Uncertainty Quantification of bcc Fe Single Crystal Plasticity," ICME 3rd World Congress, Colorado Springs, CO, June 3, 2015 (invited). McDowell, D.L., "Rectifying Bottom-Up and Top-Down Uncertainties in Multiscale Modeling: Scientific and Engineering Aspects Relevant to ICME Multilevel Materials Design and Development," ICME 3rd World Congress, Colorado Springs, CO, June 4, 2015 (plenary).

Suggested Future Directions

As stated in this report we anticipate that this foundational three-year NEAMS program will lead to multiple PhD theses in the next two years that flesh out the three multiscale uncertainty sub-problems discussed in this final report. This activity will have substantial impact on both model form/structure and parameter uncertainty in multiscale model chains, which heretofore has been relatively uncharted territory. We anticipate that a growing relationship between Georgia Tech and Sandia will also allow us to continue to develop and extend these concepts and approaches to more complex multiscale and multiphysics modeling/experiment (bottom-up and top-down) scenarios through collaboration.

The team has some additional specific thoughts regarding future research directions:

- Looking beyond Fe to hcp Zr and Zr-Nb alloys
- Understanding UQ and sensitivity to parameter choices in MOOSE based codes (MOOSE: framework used by INL for fuel performance codes)

- Extend the combined top-down and bottom-up approach to study other aspects of fuel-clad performance including fuel thermal conductivity and fission gas evolution in nuclear fuel
- Further exploration of Bayesian Approaches for multiscale model validation with imprecise probability measures

Clearly, it is important to continue to support development of systematic uncertainty methods to quantify model structure uncertainty and propagation across model chains. PI/PD D. McDowell served on a TMS Study Group in 2014-2015 which produced a roadmapping study report for multiscale modeling (<http://www.tms.org/multiscalestudy/>) that features uncertainty quantification and propagation as a primary scientific challenge to be addressed by the community (see below).

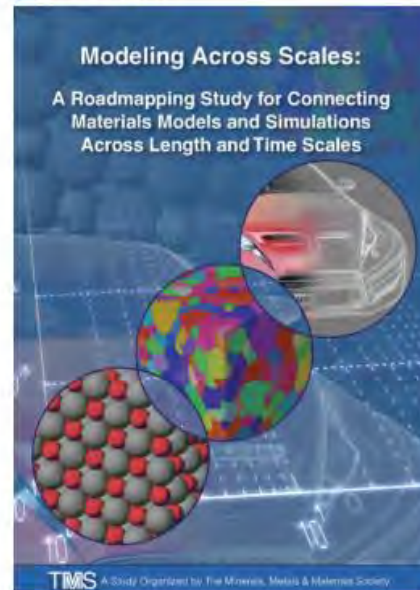
2015 TMS Study Group Report

Modeling Across Scales: A Roadmapping Study for Connecting Materials Models and Simulations Across Length (and Time) Scales

A Study Organized by The Minerals, Metals & Materials Society **TMS**

On behalf of National Institute of Standards (NIST) Material Measurement Laboratory

- Recommendation #2: Devise methods and protocols for taking into account rare events and extreme value statistical distributions.
- Recommendation #3: Develop initiatives that address uncertainty quantification and propagation (UQ/UP) across multiple models describing a range of material length and time scales.
- Recommendation #7: Develop a suite of community physics-based analysis tools (including standard protocols for performing spatial correlations and statistics)



References

- [1] Frigg, R., Hartmann, S., "Models in Science", *The Stanford Encyclopedia of Philosophy* (Fall 2012 Edition), Edward N. Zalta (ed.), URL = <<http://plato.stanford.edu/archives/fall2012/entries/models-science/>>.
- [2] M. S. Morgan and M. Morrison, *Models as Mediators: Perspectives on Natural and Social Science*. Cambridge University Press, 1999.
- [3] M. Bunge, "A General Black Box Theory," *Philos. Sci.*, 30(4), 1963, pp. 346–358.
- [4] P. Gaganis, "Model calibration/parameter estimation techniques and conceptual model error," in *Uncertainties in Environmental Modelling and Consequences for Policy Making*, P. C. Baveye, M. Laba, and J. Mysiak, Eds. Springer Netherlands, 2009, pp. 129–154.
- [5] M. R. Wigan, "The fitting, calibration, and validation of simulation models," *Simulation*, 18(5), pp. 188–192, May 1972.
- [6] M. Hofmann, "On the Complexity of Parameter Calibration in Simulation Models," *J. Def. Model. Simul. Appl. Methodol. Technol.*, vol. 2, no. 4, pp. 217–226, Oct. 2005.
- [7] A. W. F. Edwards, *Likelihood*. CUP Archive, 1984.
- [8] D. J. Bacon, Y. N. Osetsky and Z. Rong, "Computer simulation of reactions between an edge dislocation and glissile self-interstitial clusters in iron", *Philosophical Magazine*, vol. 86, no. 25–26, pp. 3921–3936, Sep 2006
- [9] Yu. N. Osetsky, A. Serra, B. N. Singh and S. I. Golubov, "Structure and properties of clusters of self-interstitial atoms in fcc copper and bcc iron", *Philosophical Magazine*, vol. 80, no. 9, pp. 2131-2157, 2000
- [10] B.D. Wirtha, G.R. Odette, D. Maroudas and G.E. Lucasa, "Dislocation loop structure, energy and mobility of self-interstitial atom clusters in bcc iron", *Journal of Nuclear Materials*, vol. 276, pp. 33-40, 2000
- [11] D. Terentyev, P. Grammatikopoulos, D.J. Bacon, Yu. N. Osetsky, "Simulation of the interaction between an edge dislocation and a <100> interstitial dislocation loop in α -iron", *Acta Materialia*, vol. 56, pp. 5034–5046, 2008
- [12] G.J. Ackland, D.J. Bacon, A.F. Calder and T. Harry, "Computer simulation of Point Defect Properties in dilute Fe-Cu alloy using a many-body interatomic potential", *Philosophical Magazine. A*, vol. 75, pp. 713-732, 1997
- [13] M.I. Mendeleev, S. Han, D.J. Srolovitz, G.J. Ackland, D.Y. Sun, and M. Asta, "Development of new interatomic potentials appropriate for crystalline and liquid iron", *Philosophical Magazine*, vol. 83, pp. 3977-3994, 2003
- [14] L. Proville, D. Rodney, M.C. Marinica, "Quantum effect on thermally activated glide of dislocations", *Nature Materials*, vol. 11, pp. 845–849, 2012
- [15] R. Groger, A.G. Bailey, V. Vitek, *Acta Mater* 2008, 56, (19), 5401-5411.
- [16] R. Groger, V. Racherla, J.L. Bassani, V. Vitek, *Acta Mater* 2008, 56, (19), 5412-5425.
- [17] J.L. Bassani, K. Ito, V. Vitek, *Materials Science and Engineering A* 2001, 319, 97-101.
- [18] S. Narayanan, D.L. McDowell, T. Zhu, "Crystal Plasticity Model for BCC Iron Atomistically Informed by Kinetics of Correlated Kinkpair Nucleation on Screw Dislocations," *Journal of the Mechanics and Physics of Solids*, Vol. 65, 2014, pp. 54-68.
- [19] A. Patra and D. L. McDowell, "Crystal plasticity-based constitutive modelling of irradiated bcc structures," *Philosophical Magazine*, vol. 92, no. 7, 2012. pp. 861–887.
- [20] A. Patra, T. Zhu, D.L. McDowell, "Constitutive equations for modeling non-Schmid effects in single crystal bcc-Fe at low and ambient temperatures," *Int. J. Plasticity*, Vol. 59, 2014, pp. 1-14.